Cross-Cutting Activities 2016 on Wind Turbine Noise, Summary Report

Bertagnolio, Franck; Aagaard Madsen , Helge; Fischer, Andreas; Kelly, Mark; Shen, Wen Zhong; Mikkelsen, Torben Krogh; Sørensen, Steen Arne; Schmidt Paulsen, Uwe; Hansen, Per; Enevoldsen, Karen

Total number of authors:
18

Publication date:
2017

Document Version
Publisher's PDF, also known as Version of record

Cross-Cutting Activities 2016 on Wind Turbine Noise

Summary Report

DTU Wind Energy E-Report-0140

January 2017

Danmarks Tekniske Universitet

Cross-Cutting Activities 2016 on Wind Turbine Noise, Summary Report

DTU Wind Energy E-Report-0140
2017

Af
Franck Bertagnolio (Editor)
Authors and Contributors: Franck Bertagnolio, Helge Aa. Madsen, Andreas Fischer, Mark Kelly, Wen Zhong Shen, Torben Mikkelsen, Steen Sørensen, Uwe Paulsen, Per Hansen, Karen Enevoldsen, Claus Pedersen, Michael Rasmussen, Kasper Clemmensen, Emre Barlas, Andrey Sogachev, Nathan Alexander (Virginia Tech, USA), Stuart Bradley (University of Auckland, NZ), Michael Kerscher (Gfai Tech, Berlin).

Forsidefoto: [Tekst]
Udgivet af: Ledelse og Administration, Anker Engelunds Vej 1, Bygning 101 A, 2800 Kgs. Lyngby
Rekvireres: www.dtu.dk
ISSN: [0000-0000] (elektronisk udgave)
ISBN: 978-87-93549-07-4 (elektronisk udgave)

ISSN: [0000-0000] (trykt udgave)
ISBN: [000-00-0000-000-0] (trykt udgave)

Forord

This report summarizes objectives and results of the Cross-Cutting Activities (CCA) on Wind Turbine Noise conducted at DTU Wind Energy during year 2016. This CCA was divided into four work packages, each covering a specific aspect of wind turbine noise generation and/or propagation.

Roskilde (DK), January 2017

Franck Bertagnolio (Ed.)
Cross-Cutting Activities 2016 on Wind Turbine Noise, Summary Report

Indhold/Content

1. Introduction and Background 6

2. WP.1: Development of Wireless Blade Inflow Sensor 8

3. WP.2: Noise Mitigation Strategies for Wind Turbines 14

4. WP.3-A: Atmospheric Modelling of Turbine Noise Propagation 22

5. WP.3-B: Coupling of Noise Source and Propagation Models 32

6. WP.4: Development of Wireless Microphones for Sound Propagation Measurements 39

Conclusions and Perspectives 45

Summary

The goal of this report is to summarize activities that took place in year 2016 as part of the Cross-Cutting Activity on Wind Turbine Noise, self-financed by DTU Wind Energy. A short description of the background behind this project (in particular Cross-Cutting Activities conducted in year 2015), the main objectives of the various studies and scientific achievements are reported in the introduction. Then, each Work Packages constituting this project are described in more details in the following sections.

1. Introduction and Background

Cross-Cutting Activities (CCA) are research and/or development projects financed by DTU Wind Energy using internal fundings in order to promote a number of chosen topics that are considered as strategic by the management for the future of the department.

In 2015, a first CCA was initiated with focus on Wind Turbine noise. It consisted of 3 work packages (WP):

- WP1: Wireless Microphone Array
- WP2: Development of Noise Measurement and Characterization Methods
- WP3: Development of Wind Turbine Noise Prediction Tools

WP1 concentrated on the development of a new technology for which microphones are connected to mobile phones in order to ease their deployment over a larger terrain area surrounding a wind turbine or wind farm. Typically, wind turbine noise measurements rely on microphones connected with cables to an acquisition system, which inherently limits the area that can be covered by these microphones.

WP2 relied on a series of measurement campaigns of the NordTank 500/41 wind turbine located at the DTU-Risø Campus. The wind turbine is extensively instrumented (included a nearby met mast) and a series of additional sensor systems related to wind turbine noise were also developed, namely surface pressure microphones on blades to characterize aerodynamic noise sources and state-of-the-art accurate ground microphones connected with cables to measure the wind turbine noise in the near-field (i.e. at a distance of the order of the wind turbine height, similarly to the IEC 61400-11 standard for wind turbine noise measurement).

WP3 intended to carry on the development and validation of numerical tools already in progress at DTU Wind Energy, both concerning wind turbine noise generation and propagation.

The main strategy behind the above choices is that WP1 and WP3 would heavily rely on the measurement campaigns on the NordTank 500/41 wind turbine of WP2 as a mean of validation. Unfortunately, due to the small size of this turbine and the proximity of a fairly trafficked main road, wind turbine noise propagation effects could not be properly measured within this project.

This first edition of the CCA-2015 led to a series of publications in scientific journals and conference proceedings.

It was decided that CCA on Wind Turbine Noise should be continued for a second year. The present CCA-2016 consists of 4 WPs:

- WP1: Development of Wireless Balde Inflow Sensor
- WP2: Noise Mitigation Strategies for Wind Turbines
- WP3: Atmospheric Modelling of Wind Turbine Noise Propagation
- WP4: Development of Wireless Microphones for Sound Propagation Measurements

Similarly to the CCA-2015, the main idea is to use measurement campaigns on the Nordtank 500/41 turbine to support most activities. The initial plan was to use the Vestas V-52 turbine

also operating at the DTU-Risø Campus, more specifically in WP2 for experimenting mitigation strategies using the controller. Unfortunately, this proved to be impossible as the turbine was used as part of different measurement campaigns which had higher priority, and it was therefore not possible to implement noise mitigation devices or strategies at the same time on this turbine.

As mentioned earlier, an important component of the present CCA are measurement campaigns on the NordTank 500/41 wind turbine. During the CCA-2016, a total of four campaigns were conducted (a campaign was also attempted in September, but weather conditions did not permit its completion). These are:

- June 01: this campaign included measurements with a Pitot tube connected to a autonomous wireless acquisition system, surface pressure microphones on the blade, ground microphones for noise measurements in the near-field, and Wifi microphones for noise measurements in the far-field.
- October 25-27: noise mitigation add-ons were tested (finlet and brushes) together with ground microphones in the near-field. Wifi microphones were also used in the near-field for validation/calibration.
- November 07-08: surface pressure microphones and Pitot tube + wireless acquisition system were tested again in order to solve problems identified during the June campaign.
- November 14: Gfai Tech (German acoustic camera manufacturer) and Stuart Bradley (University of Auckland) visited DTU-Risø Campus and performed tests on the Nordtank 500/41 turbine using noise sources attached to one of the blade. Noise measurements were conducted in the near-field using an acoustic camera brought by Gfai Tech.

The main objectives and achieved results for each of the four WPs are detailed in this report in Sections 2 to 5. In Annex A, a GANTT chart summarizing the different work packages' activities and an overview of the budget is provided. The main deliverables and milestones are also provided in a separate figure.

2. WP.1: Development of Wireless Blade Inflow Sensor

WP Manager: Helge Aa. Madsen
Participants: Uwe Paulsen, Franck Bertagnolio, Andreas Fischer, Per Hansen, Claus Pedersen, Michael Rasmussen, Kasper Clemmensen

Objectives

In this work package, the main goal is to continue and improve the development of a wireless inflow sensor, which consists of a Pitot tube attached to a device that is attached to the blade and which is capable to acquire data from this Pitot tube wirelessly. This set-up was initially developed and tested during the CCA on Wind Turbine Noise in year 2015. As part of the present WP, it was intended to connect surface pressure (SP) microphones (see below) to the acquisition device but this could not be achieved so far.

In addition, the SP microphones set-up (using dedicated microphones purchased from G.R.A.S Sound & Vibration A/S) used to characterize the aerodynamic noise sources directly on the blades proved to be malfunctioning in many instances during the CCA-2015. Therefore, new tests of this technological set-up are performed as part of the present WP to clarify these issues. In particular, meetings with GRAS engineers were organized and they tried to improve their microphones' technology to fit to our requirements (it is believed, but still very hypothetical, that the blades constantly changing altitude due to the rotation of the blades act as a pump due to the change in atmospheric pressure, resulting in an accumulation of water vapor into the microphone's interior cavity). In addition, after discussions with Brüel & Kjær (who also manufactures such dedicated SP microphones), it was agreed that we could borrow one of their microphones for testing.

The main steps of this WP are the following:

1. The Pitot tube and wireless acquisition system are tested. Calibration of the Pitot tube to obtain the angle of attack onto the blade section has been conducted in a small open jet wind tunnel. The methodology and results are found in Moñux & Paulsen (2016).
2. Concerning the SP microphones, the set-up was tested in two occasions.

These main results of these investigations are discussed separately below.

Main Results Concerning Wireless Pitot Tube Sensor

The inflow sensor device (see Figure 1) was tested during measurement campaigns on May 30-June 01 and November 07-08. The experiment failed during the first campaign after some time (between 20 mins and 1 hour) as the sensor detached (most probably because the gluing process failed to securely attach the device on the blade). The data recorded before failure could still be recovered. During the second experiment, the device was attached by drilling

holes into the blade and using screws to fix it to the blade. This second option proved successful and data were acquired during the full length of the experiment.

Figure 1 - Pitot Tube Inflow Sensor

The results are the following. The next step in this study is to extract information about the angle of attack (AoA) impinging the blade at the device location from the two campaigns. Figure 2 shows a 325 second long record of the local speed obtained with two different pitot tubes (#1 was destroyed). The spectral resolution is detailed as shown in the Welch spectra.

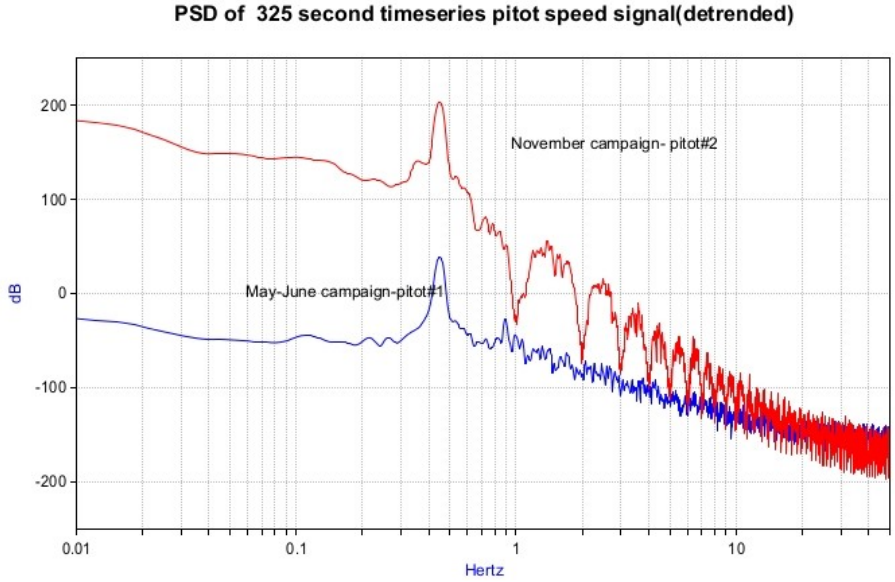

Figure 2 - Spectra of measured Inflow Velocities

Main Results Concerning Surface Pressure Microphones Sensors

The SP microphones were tested during two measurement campaigns (May 30-June 01 and November 07-08). Typical mounting of the microphones is illustrated in Figure 3.

Figure 3 - Surface Pressure Microphone on Blade

Comparisons have been performed between SP measurements and the HAWC2-Noise model developed during CCA-2015 (combining aerodynamic modelling using HAWC2 and various noise generation models for the acoustic emission). The averaged angle of attack on the blade is computed for a specific mean wind speed using HAWC2. The TNO trailing edge noise model is used to predict surface pressure measurements from a microphone located near the trailing edge. Results are displayed in Figure 4. It can be seen that the model reproduce the main tendencies of the measured data, however with quite large qualitative discrepancies. The transition parameter Ncrit (as part of the e^N transition model in CFD) has a significant influence on results at lower angles of attack. Th recent improvement of the TNO model by Fischer *et al*. (2017) seems to improve results in particular at high velocities (i.e. higher angles of attack of the airfoil relative to the inflow).

Concerning the mal-functioning sensors, 3 microphones out of the 6 GRAS microphones failed during the June 01 experiment. Therefore, it was decided to test them again and compare measurements against a similar microphone borrowed from Brüel & Kjær (although it should be noted that the B&K microphone as a membrane twice as large as the GRAS ones, which was the reason why it was originally decided to purchase GRAS microphones instead of B&K's) during the November 07-08 campaign.

Figure 5 shows the spectra (for the GRAS SP microphone ref.203397) at specified times. At 04:42 (and before, since the start of the experiment) it is not functioning properly. At 04:46 it is functioning (and then it remains until the end of the experiment). The records of 04:44 include on/off time and the spectrum is accordingly in between. In conclusion, something quite sudden happened... Approximately 30 mins before the mic. started functioning again, there were some problems with the acquisition system for a few minutes. A closer investigation may determine if this could be related, but at least if there is a relationship, it only affected this one microphone and not the remaining ones.

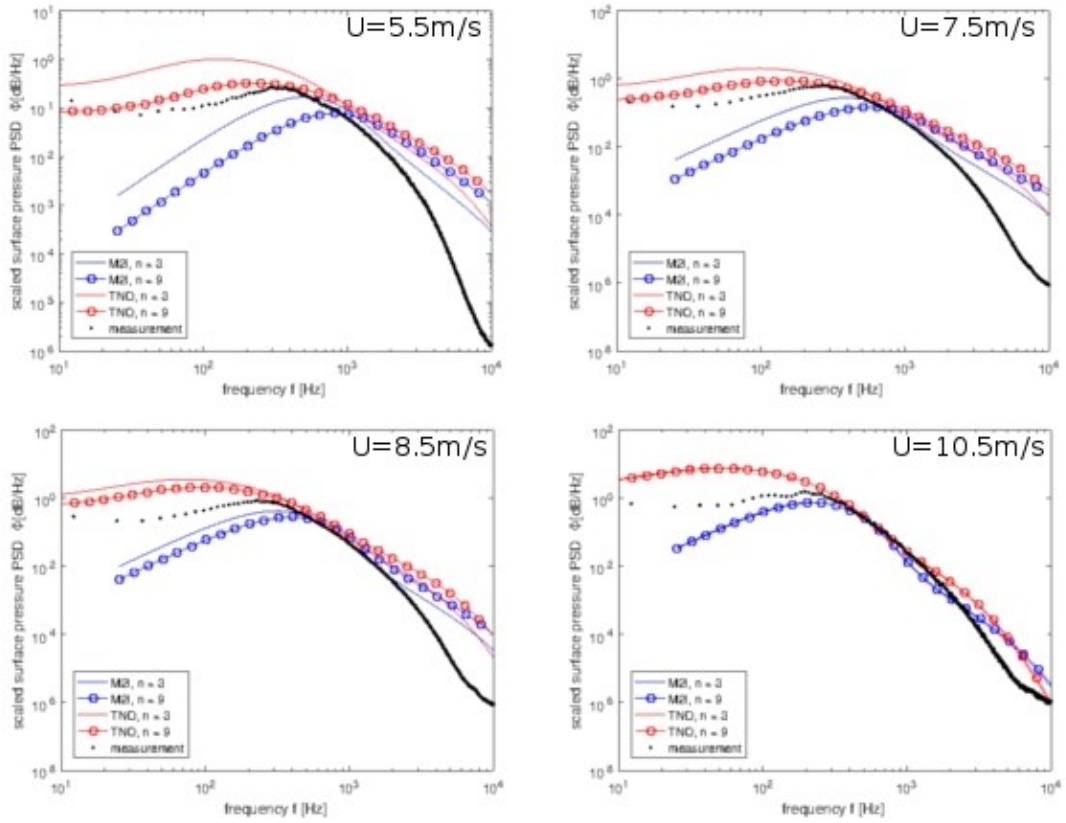

Figure 4 - Comparison of measured and modelled SP (Lines: Ncrit=3, Lines with circles: Ncrit=9, Red lines: TNO model according to Bertagnolio et al., Blue lines: TNO model according to Fischer et al.)

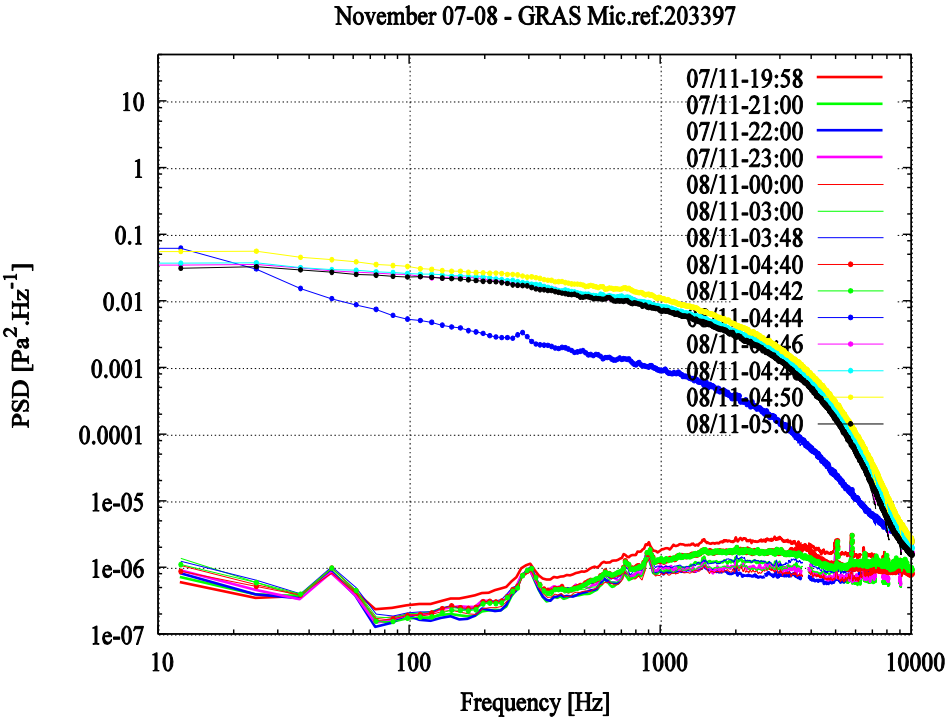

Figure 5 - SP Measurements of a GRAS Microphone (ref.203397)

The comparison between GRAS and B&K microphones is illustrated in Figure 6. It can be seen that the B&K microphone compares reasonably well with GRAS microphones, but exhibits lower spectral energy and seems to roll-off more quickly at high frequencies (2kHz-4kHz). These differences (at least the spectral roll-off) are attributed to the larger membrane (1/2" instead of 1/4" for the GRAS microphones).

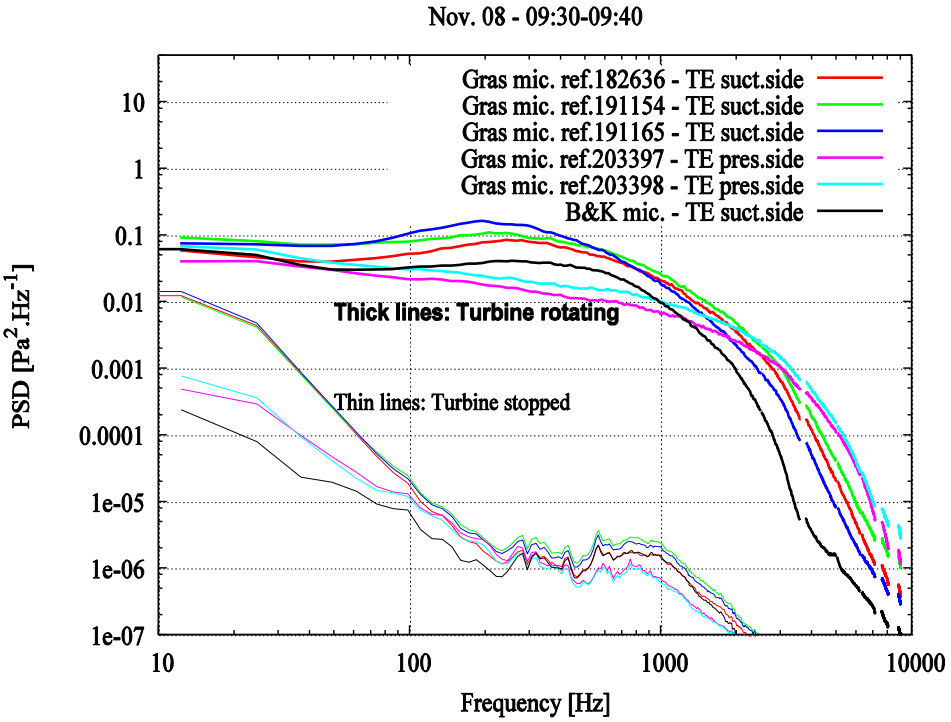

Figure 6 - Comparison between GRAS and B&K Microphones

Conclusions

The Pitot tube inflow sensor with wireless acquisition system has been further developed and tested. This technology now seems quite reliable and proved to be able to run without problem for a full night. Using more powerful battery would increase the performance of this system. A reliable calibration of the Pitot tube still needs to be performed. The next step would be to connect one (or possibly a few) SP microphone to this acquisition system and providing a satisfying sampling rate. Indeed, in contrast to the Pitot tube monitoring the inflow, the study of aeroacoustic characteristics with SP microphones require much higher sampling frequencies. This prove impossible so far with the present design of the acquisition system, but another design using a GRAS hardware system may be a future option.

Concerning the SP microphones, the mal-function of the GRAS microphones is quite erratic and it has not been possible to identify the problem with certainty... Nevertheless, when they are properly functioning, the results appear to be sensible and somehonw in agreement with the modeling approach. Further thorough study of the qualitative discrepancies between measurement and model must be conducted in order to fully exploit this technology for e.g. using these SP microphones as sensors for noise generation control and monitoring of the flow field around the blade in general.

References

Fischer A, Bertagnolio F, Madsen HAa (2016) Improvement of TNO type trailing edge noise models. *European Journal of Mechanics B - Fluids*, Vol. 61, p.255-262.

Moñux O, Paulsen US (2016) Aerial Sensor for wind turbines: Design, implementation and demonstration of the technology. *Technical Report, DTU Wind Energy E-0128 (EN).*

3. WP.2: Noise Mitigation Strategies for Wind Turbines

WP Manager: Andreas Fischer
Participants: Franck Bertagnolio, Nathan Alexander (Virginia Tech, USA), Karen Enevoldsen, Per Hansen, Michael Rasmussen, Kasper Clemmensen

Objectives

The objective of this WP was to test several noise reduction technologies on our research wind turbines. Due to availability the tests were only conducted on the NordTank wind turbine. Two add-on devices were tested: brushes and finlets. The finlets were designed and provided by Virginia Tech. The rationale behind the design of these finlets is explained in Annex B.

Experimental Set-Up

On October 26, we tested two different trailing edge noise reduction technologies, trailing edge brushes and finlets. In order to make a time efficient test, only two blades were equipped with one of the noise reduction technologies each. Blade no.1 was equipped with the brush, blade no. 2 with the finlets and blade no. 3 was kept clean to function as a reference.
The brushes cover the blade at radial position 15 m to 18 m, shown in Figure 7.

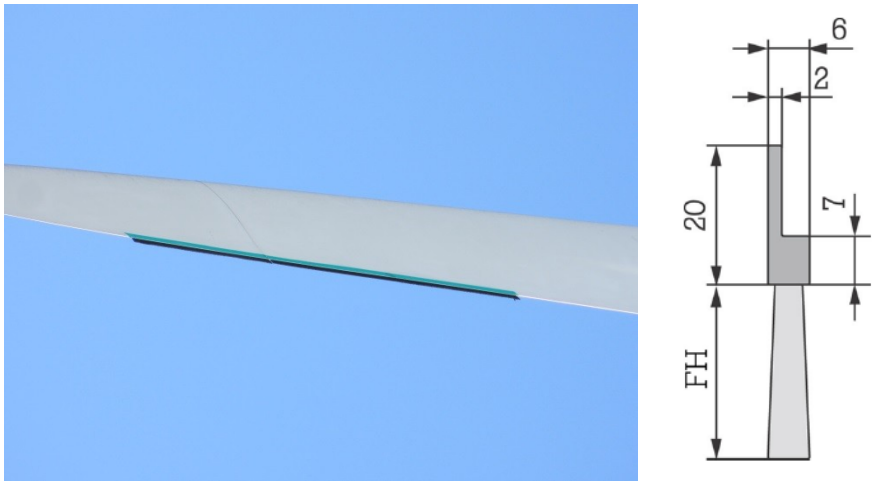

Figure 7 - Brushes installation set-up

The brushes were 40 mm long and the diameter of the hair was 0.3 mm. The brushes came in elements of 1 m length and had a skirting which is also shown in Figure 7.

The finlets were developed by Virginia Tech University and the detailed geometry is proprietary. They were about 70 mm long, but the length varied slightly with the radial position. The height

was about 8 mm, also varying with the radial position. They cover the blade at radial position 15 m to 18 m. They were mounted on pressure and suction sides as shown in Figure 8.

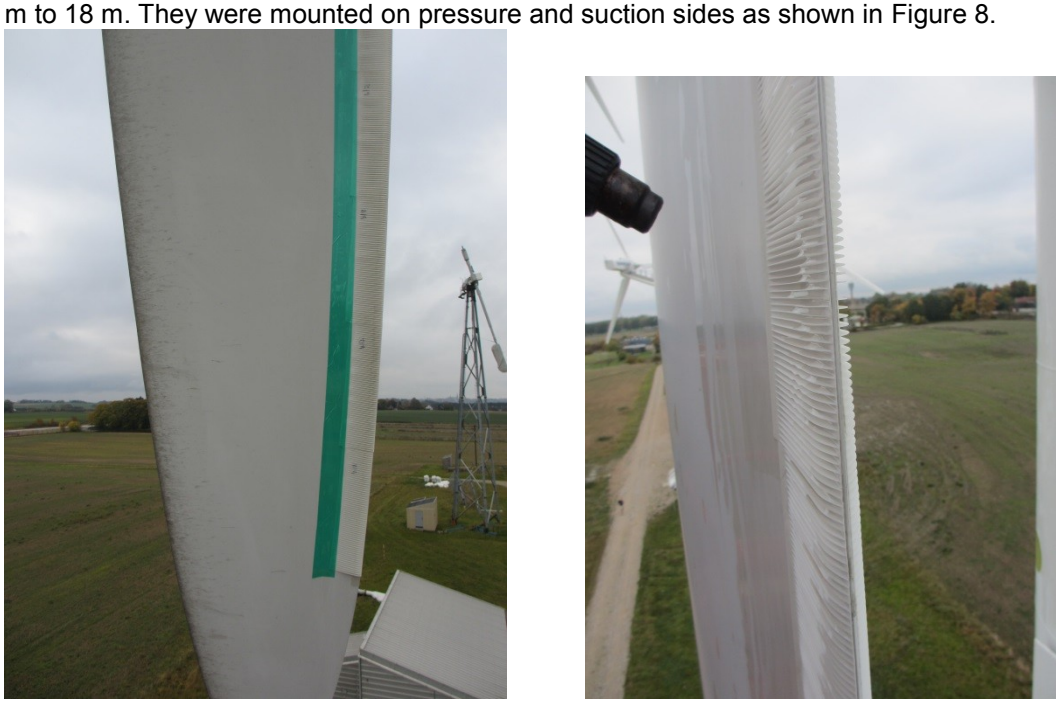

Figure 8 - Finlets installation set-up

The noise reduction characteristics were measured with a microphone that was placed approximately at the down-stroke position as shown in Figure 9.

Figure 9 - Ground microphone below blades' down-stroke position

The position of the microphone was 7.8 m easting and -10.5 m northing relative to the centre of the tower. The positioning accuracy of the microphones was approximately +/-1 m.
On October 27, the noise mitigation technologies were removed to make a reference measurement with 3 clean blades. The wind direction had changed and the wind turbine adjusted its ori-

entation by yawing. The position of the down-stroke measurement was changed to follow the yaw movement of the turbine. The position on this day was -0.5 m easting and -13.3 m northing.

Main results

The measurement at 17:00 on October 26 was analysed to investigate the effect of the noise reduction technologies. The wind profile and turbulence intensity as 10 minutes average are shown in Figure 10.

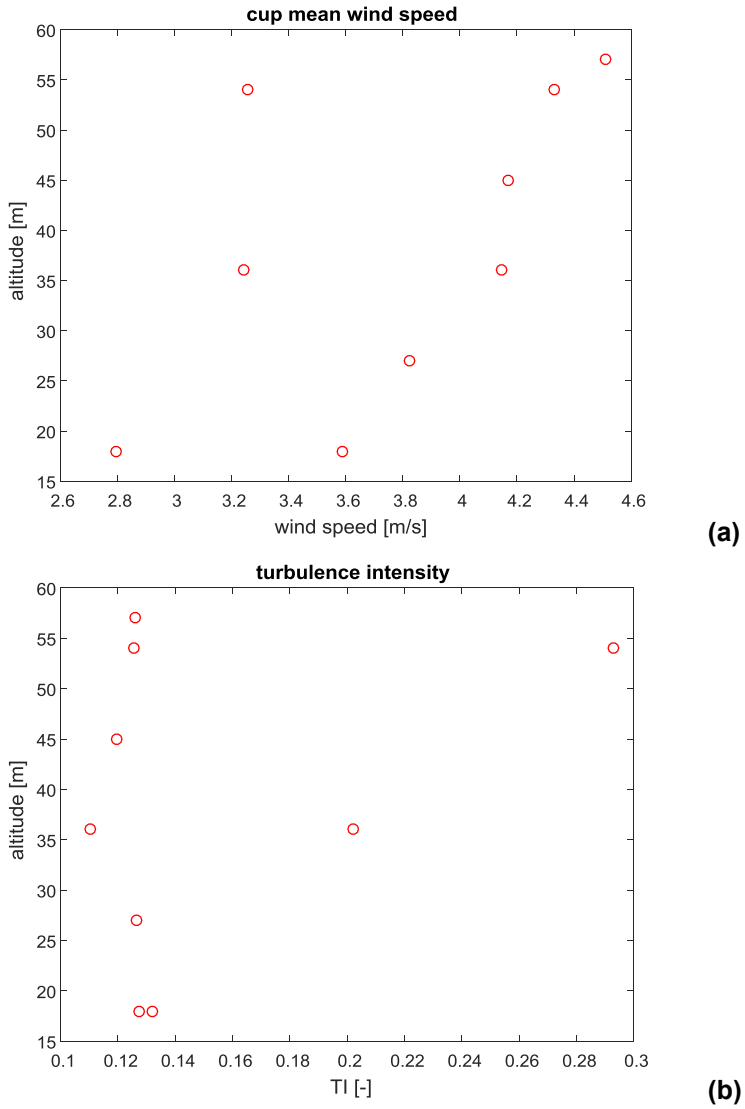

Figure 10 - Wind speed (a) and turbulence intensity (b) profiles when testing noise reduction devices

The southern cup anemometers measured higher velocities and lower turbulence intensities, because the main wind direction was from the south. The northern anemometers were in the wake of the met mast. The yaw angle of the turbine was 202 degrees.

The spectrogram of the signal measured with the down-stroke microphone as function of the azimuth angle of blade 1 for several 2 minutes time series was evaluated. The azimuthal resolution was 15 degrees. For the time series starting at 17:02 it is shown in Figure 11.

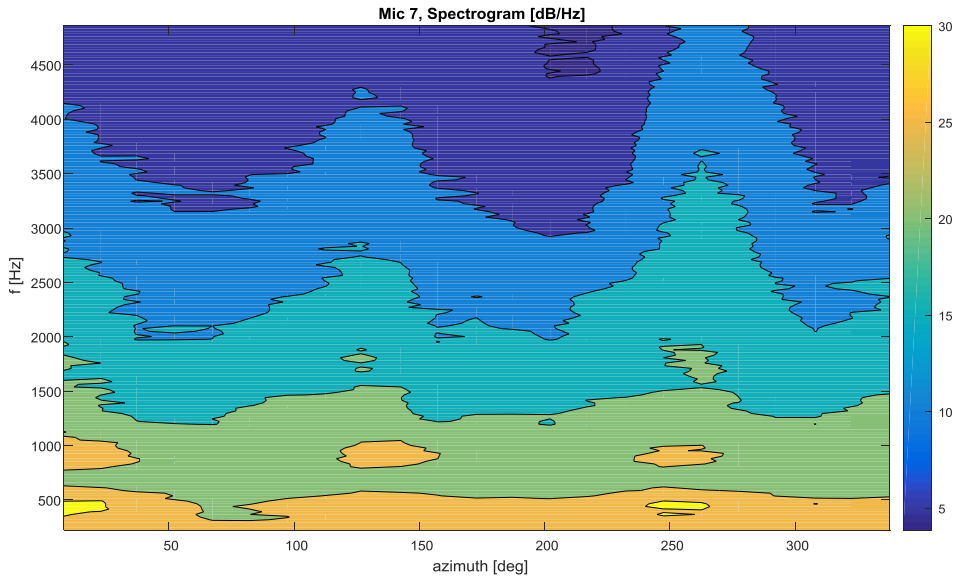

Figure 11 - Spectrogram of blade passages with/without noise reduction devices

The 3 blades can be clearly distinguished in the spectrogram. The noise signature of blade 1 (brushes) is found at the azimuth between 120 and 140 degrees, blade 2 (finlets) between 240 and 260 degrees and blade 3 (clean) between 0 and 20 degrees. The azimuth position at which the spectrum reaches its maximum is slightly dependent on the frequency. It is roughly separated by 120 degrees as one would expect. Blade 2 equipped with finlets appears to be louder than the other blades.
In order to get better quantitative data the 1/3 octave band spectra at distinct azimuth positions were investigated, and displayed in Figure 12.

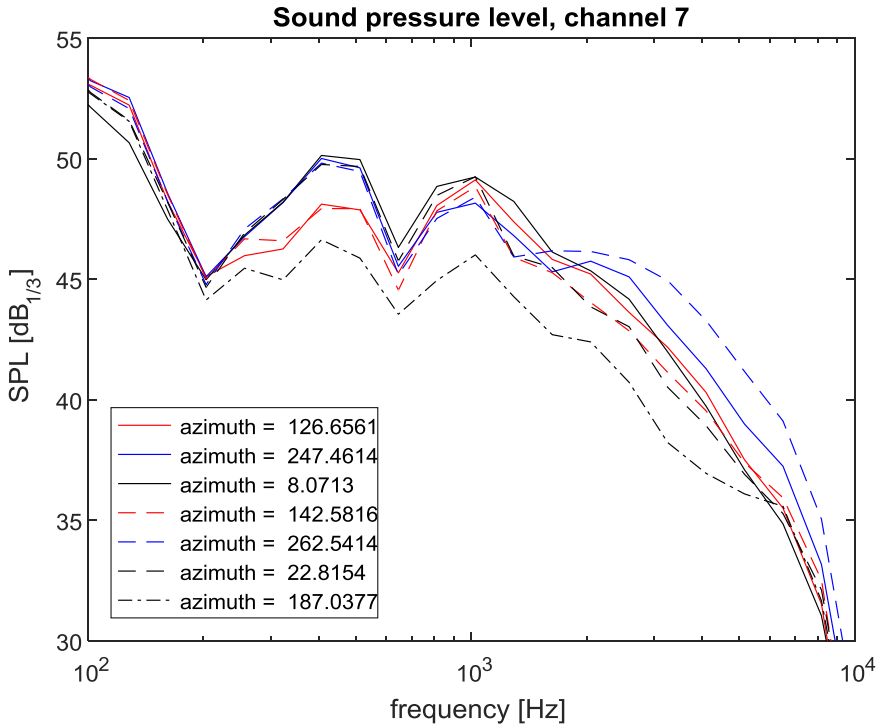

Figure 12 - Sound pressure spectra of blades with/without noise reduction devices

The noise signature of blade 1 (brushes) is defined by the two red lines, the one of blade 2 (finlets) by the blue lines and the one of blade 3 (clean) by the black lines. The black dash dot line shows the spectrum were the noise signature from none of the blades is measured. It can be considered as a background noise level. In the frequency range between 200 and 700 Hz the blade with brushes is up to 2 dB quieter than the other two blades which are equally loud. This is very surprising, because previous noise computations showed that turbulent inflow noise should be dominant in this frequency range and not trailing edge noise. In the other frequencies the blade with brushes is equally loud as the clean blade. The blade with finlets is up to 1 dB quitter in the frequency range between 600 and 2000 Hz than the two other configurations, but it is up to 4 dB louder in the frequency range above 2000 Hz.

The same analysis is carried out for the reference case with 3 clean blades. The atmospheric conditions were slightly different as shown in Figure 13.

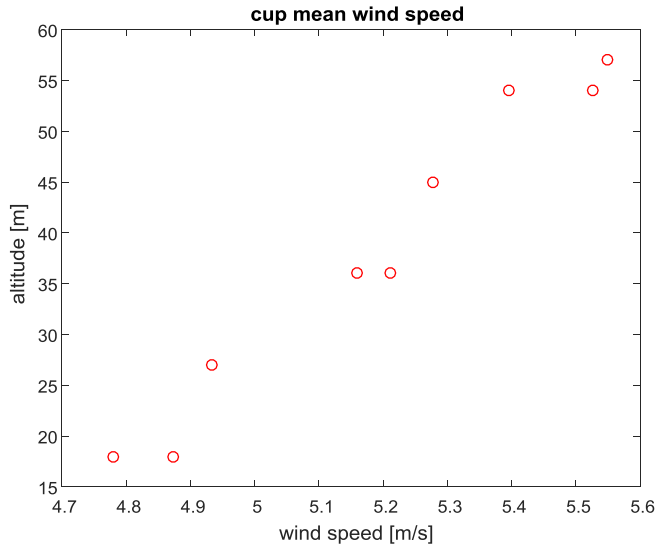

(a)

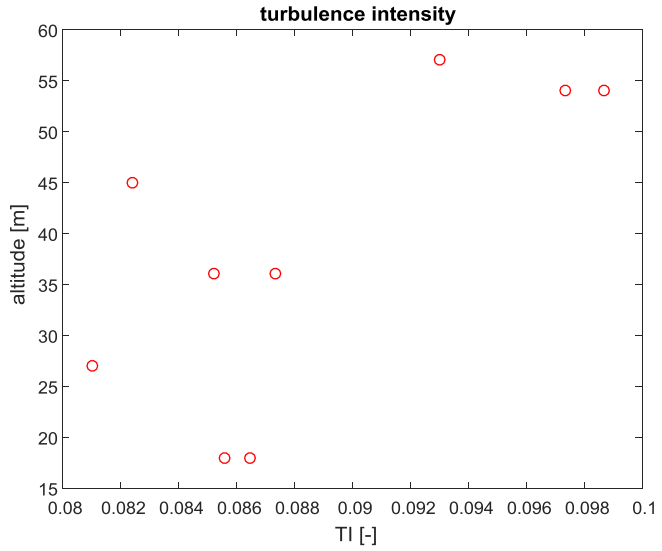

(b)

Figure 13 - Wind speed (a) and turbulence intensity (b) profiles when testing three clean blades

There is a higher shear and the wind speed is in average also higher. The wind direction has changed. The yaw position of the turbine was 271 degrees. Hence, it is only possible to compare the two situations relatively.
The spectrogram of the 2 minutes time series starting at 12:02 measured with the down-stroke microphone is shown in Figure 14.

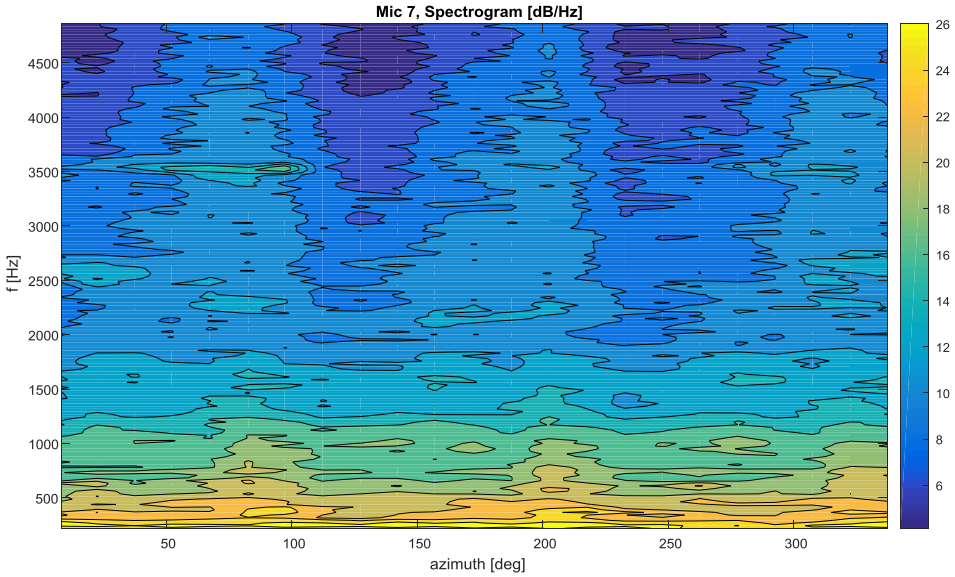

Figure 14 - Spectrogram of three clean blades passages

The 3 blades show a very similar noise signature. The background noise is higher than for the October 26 measurement. The noise signature of the blades does not stand out so clearly. The azimuth angles where the maximum levels are reached have shifted. This is probably due to a change of the down-stroke microphone position relative to the blade. The noise levels are also influenced by the change in relative position.
The 1/3 octave spectra at selected azimuth angles are shown in Figure 15.

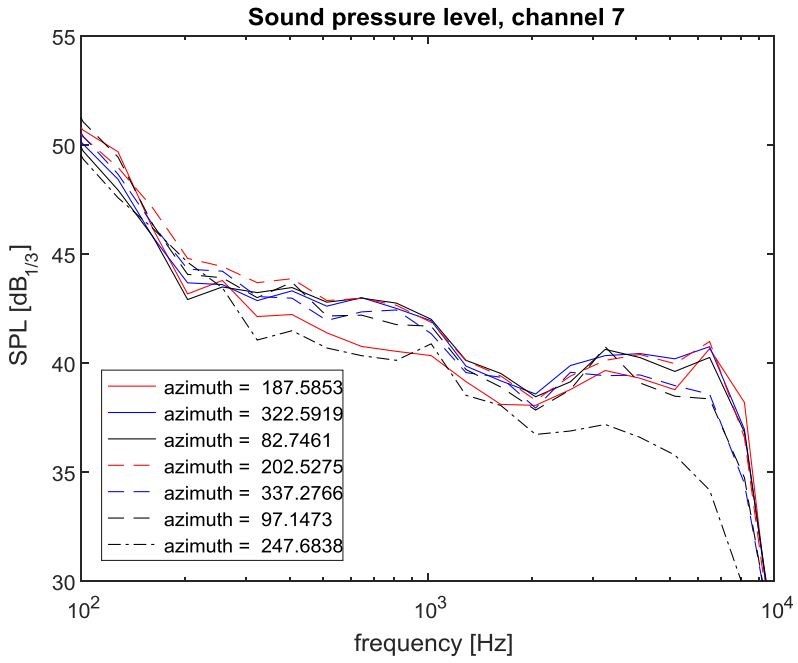

Figure 15 - Sound pressure spectra of three clean blades

The noise signature of the 3 clean blades is within 1 dB. Hence, the difference in the noise signature observed with the add-ons is larger than the measurement uncertainty.

Conclusions

The brushes showed a noise reduction of up to 2 dB in 1/3 octave bands in the frequency range between 200 and 700 Hz. In the other frequencies it was equally loud as the clean blade. The finlets reduced the noise by up to 1 dB in the frequency range between 600 and 2000 Hz, but there was an increase of up to 4 dB in the frequency range above 2000 Hz. Overall the blade with finlets was louder than the clean blade, especially if A-weighting is applied.

4. WP.3-A: Atmospheric Modelling of Turbine Noise Propagation

WP Manager: Mark Kelly
Participants: Mark Kelly, Emre Barlas, Andrey Sogachev, Wen Zhong Shen

Objectives

The primary goal of work package 3 (WP3) was to usefully and reasonably characterize the propagation of noise from a single turbine, as affected by its wake and environmental conditions. This is accomplished via a probabilistic model, which relies on output from a parabolic-equation ("PE") acoustic propagation model, which was in turn driven by an atmospheric boundary-layer ("ABL") flow model that solves the Reynolds-Averaged Navier Stokes ("RANS") and temperature equations.

4.1 Combined modelling of atmospheric turbine-noise propagation

The basis for the acoustic propagation modelling is the parabolic equation (PE) method, with a 2-dimensional implementation and solver as outlined in Barlas *et al.* (2016). This solver, which can also account for temperature-induced sound-speed profile deviations (Barlas *et al* 2017), is driven by 2-D wind fields generated for different atmospheric stability regimes by an atmospheric boundary-layer (ABL) flow model. The atmospheric flow fields are calculated using the Reynolds-averaged Navier-Stokes (RANS) flow solver "ScaDis" of Sogachev (2002) that includes a self-consistent atmospheric stability formulation within the k-epsilon turbulence modeling (Sogachev & Kelly 2012). The mean flow is calculated including the wake effect, via an actuator disc implementation in ScaDis; this is done because the *combined effect* of atmospheric stability and the turbine wake *on the flow* is crucial in calculating the environmental propagation of turbine noise. The latter is primarily due to the fact that the mean sound speed profile $c(z)$ is dominated by the mean wind profile $U(z)$ as affected by stability (surface flux), with the temperature profile playing only a minor role.

In order to arrive at meaningful turbine-noise propagation statistics, e.g. mean sound loss over distance, we start by attempting to account for the statistical behavior of the primary variable characterizing the (aggregate) atmospheric effect on turbine-to-ground propagation: the Obukhov length. In particular, the inverse Obukhov length, $L^{-1} = -\kappa(g/T_0)\,H/u_*^3$, defined by fluxes of heat (H) and momentum (u_*^3) in the surface layer (~10-30m above ground), is a direct measure of the atmospheric stability. Further, its distribution $P(L^{-1})$ tends to follow a universal form that is effectively scalable from site to site, as found by Kelly & Gryning (2010); this form has been shown to predict the mean profile $U(z)$ at various sites (Kelly & Troen 2016). The wind profile dominates the sound speed profile, so effect of stability on the sound speed profile is through the wind shear, particularly approaching receivers near ground; since we know the range of L^{-1} to be expected across (typical) turbine sites in practice, then knowing the form $P(L^{-1})$ allows us to sample a number of L^{-1} and calculate the propagation for each. Specifically, we simulate the flow field—including turbine-induced wake—for a representative range of stability cases, calcu-

late the propagation loss for each case, and then we are able to make a weighted sum of the case results based on the widths of the unstable ($L^{-1} < 0$) and stable ($L^{-1} > 0$) sides of the stability distribution $P(L^{-1})$.

4.1.1 Probabilistic model: atmospheric characterization for sound propagation

The stability distribution for the nearby Lille Valby site is shown in Figure 4-1, calculated from 2 years of sonic-anemometer measurements taken at 10 m above ground. This is typical for mid-latitude sites, and can also be taken to represent the climatological conditions for the site of the Risø turbine noise measurement campaign.

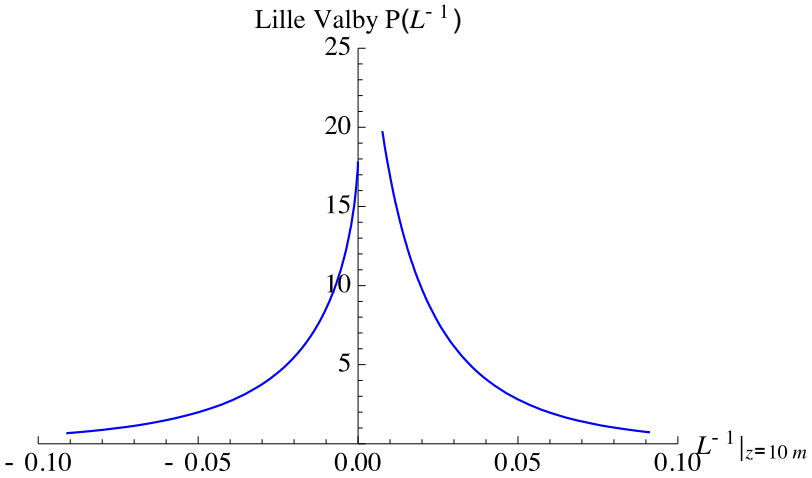

Figure 4-1. Distribution of stability (inverse Obukhov length) for local (Lille Valby) site; units on *x*- axis are m^{-1}. Shaded/red: observations; blue line is universal distribution (Kelly & Gryning, 2010).

For our study, we selected 15 stabilities spanning the distribution shown in Figure 4-1, including the neutral case of $L^{-1} = 0\ m^{-1}$. While Barlas *et al* (2017) calculated propagation results for only a significantly stable and unstable case, here we address the need to model the various propagation conditions over the range of stabilities. This is necessary because sound attenuation can be most significantly reduced for slightly- to modestly-stable cases, particularly at distances greater than 1km from a turbine; i.e., the most stable cases do not cause the loudest signals at long distances. Less stable high-wind conditions, which can happen more frequently, can enhance propagation, as can ABL depths that tend to occur in such conditions.

A basic probabilistic model is devised here, which allows estimation of low-order statistics of turbine noise propagation (loss) due to the ABL. The simplest form of the model is the discretized version of calculating the average sound pressure loss (ΔSPL) over all stabilities, analogous to means of profiles *U*(z) as in Kelly & Troen (2016),
i.e. $\Delta SPL(r,f) = \int \Delta SPL(r,f|L^{-1})\ P(L^{-1}) dL^{-1}$. This is a function of frequency *f* and distance from source *r*, as well as height above ground and angle from mean wind direction; however, we do not (yet) consider the last two aspects and thus suppress them here in the notation. The integral can be approximated by a sum, sampling the stability distribution $P(L^{-1})$; in other words it is a weighted average:

$$\Delta SPL(r,f) = \sum_i a_i P(L_i^{-1})\, \Delta SPL(r,f|L_i^{-1}). \quad (4.1)$$

Here a_i is the weight for each case, proportional to $P(L_i^{-1})$ and the L^{-1}-space sampling interval. The 2-sided stability distribution is modelled as

$$P_{\pm}(L^{-1}) = \left[n_{\pm}/\Gamma\left(\tfrac{5}{2}\right)\right](C_{\pm}/\sigma_{\pm}) \exp\left[-(|L^{-1}|C_{\pm}/\sigma_{\pm})^{2/3}\right] \quad (4.2)$$

where $\sigma_{\pm}$ are the variability[1] in L^{-1}, $\{C_+, C_-\} = \{1{,}3\}$, $n_+ = (1 - n_-)$ is the fraction of conditions which are stable ($L^{-1} > 0$); "+/-" subscripts indicate values for either stable or unstable conditions (see Kelly & Gryning 2010). The width of $P(L^{-1})$ for stable and unstable conditions (σ_+, σ_-) and the fraction n_+ determine the distribution, so for a given $\{n_+, \sigma_+, \sigma_-\}$ we can calculate $P(L^{-1})$, and from it the a_i, from a limited number of RANS and PE simulations.
Thus we choose 15 stability cases which span the range stabilities encountered 98% of the time on the stable side for Lille Valby, giving priority/weight to stable conditions (smaller sampling interval)—because L^{-1} has a greater effect on *U*(*z*) and *SPL* in stable conditions, and because unstable conditions have an effect which does not vary much with L^{-1} and which saturates for more negative L^{-1} (i.e. the atmosphere is well mixed for any cases more unstable than the minimum value we chose). The stabilities chosen are

$L_i^{-1} = \{-12.3, -9.5, -7.7, -5, -3.5, -2.3, -1.6, 0, 9.7, 12.7, 19.2, 23.2, 32.1, 46.5, 67.8\}$ km^{-1}.

4.1.2 Atmospheric CFD Flow Model

The ScaDis flow model is a RANS solver employing a two-equation turbulence closure scheme (Sogachev 2002), including a self-consistent atmospheric stability formulation which gives results satisfying Monin-Obukhov theory (Sogachev & Kelly 2012). The code includes the effect of the Coriolis force as well as cloud cover (radiation), and reproduces both the diurnal cycle as well as associated ABL depth variations. It was run in 2-D mode with 10 m resolution, using the $k - \epsilon$ equations for turbulence closure. Diurnal cycles were run with various geostrophic winds (8, 10, 12, 14 m/s) in clear conditions, and 50% and 100% cloud cover conditions were also run for U_G=10 m/s. In aggregate, 15 simulation cases were taken, which span the range of stabilities as mentioned above in section 4.1.1.

Two sample mean flow fields are shown in Figure 4-2, corresponding to (a) mildly stable conditions with $L^{-1} = 0.013$ m^{-1} (i.e. higher wind speeds at turbine rotor heights) common during nights and winter; and (b) weakly unstable conditions with $L^{-1} = -0.012$ m^{-1}, commonly found during sunny or partly-cloudy days. One can see these are relatively common by noting that the values of 1/*L* are near the peak region of $P(L^{-1})$ shown in Figure 4-1 above. The flow fields were generated using ScaDis, for different geostrophic (driving) wind speeds, above a uniform grass roughness (z_0=3 cm) and flat terrain. The turbine rotor is located at *x*=0 from heights *z*=50 m to *z*=150m above ground level, and is simulated using the common actuator disc method. One can see the effect of stability on both the wind profile upwind of the turbine, as well as upon the wake recovery, from Figure 4-2. In the wake, the stability affects the "competition" between recovering ambient high shear and turbulent mixed flow, and the distance over which these effects (and the flow) equilibrate.

[1] The variability in stability is $\sigma_{\pm} = (g/T_0)\langle(\overline{w\theta} - \langle\overline{w\theta}\rangle_{\pm})^2\rangle^{1/2}\langle u_*\rangle_{\pm}^{-3}$; see Kelly & Gryning (2010) for more detail.

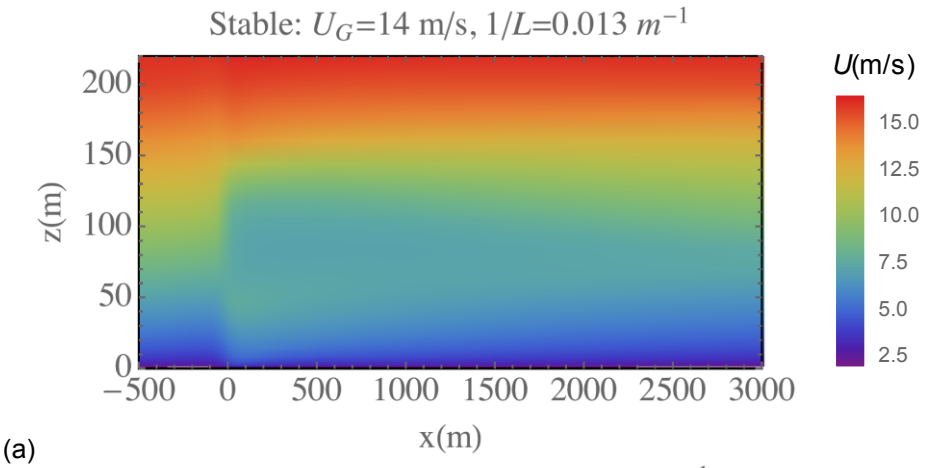

(a)

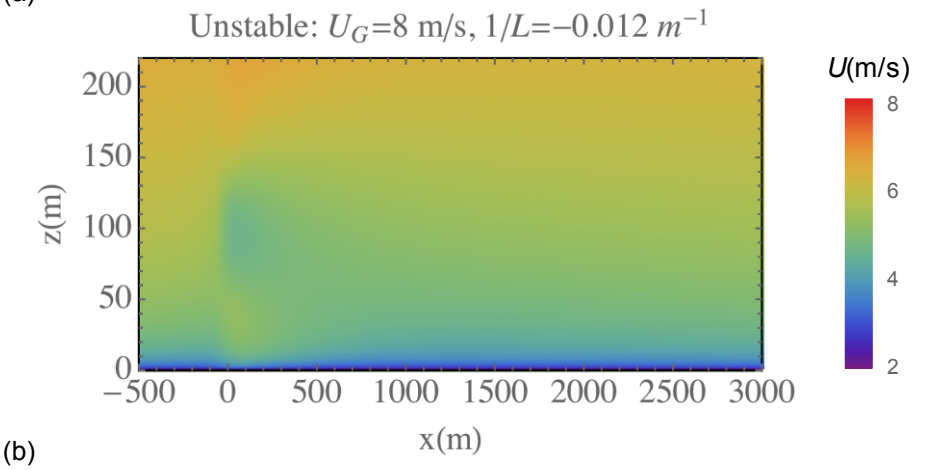

(b)

Figure 4-2. Input wind fields for weakly stable and unstable regimes, produced by ScaDis.

Another stability-related aspect of the ABL that affects the flow and propagation, which is implicitly incorporated in our probabilistic model (4.1) via ScaDis, is the ABL depth h_{ABL}. In the cases shown in Figure 4-2, h_{ABL}>250m, but for more stable conditions the ABL can be shallower than 200m (or even 100m in more extreme cases). ScaDis captures the stability-affected depth by simulating the evolving ABL, as well as cloud cover (which causes more neutral conditions and also affects h_{ABL}). For example, the most stable case simulated ($L^{-1} = 0.068$ m^{-1}) had a depth h_{ABL}~100m and associated mean 'jet' spanning part of the rotor, resulting in negative shear in the wake of the rotor; the flow field from this rarest of simulated cases is shown in Figure 4-3.

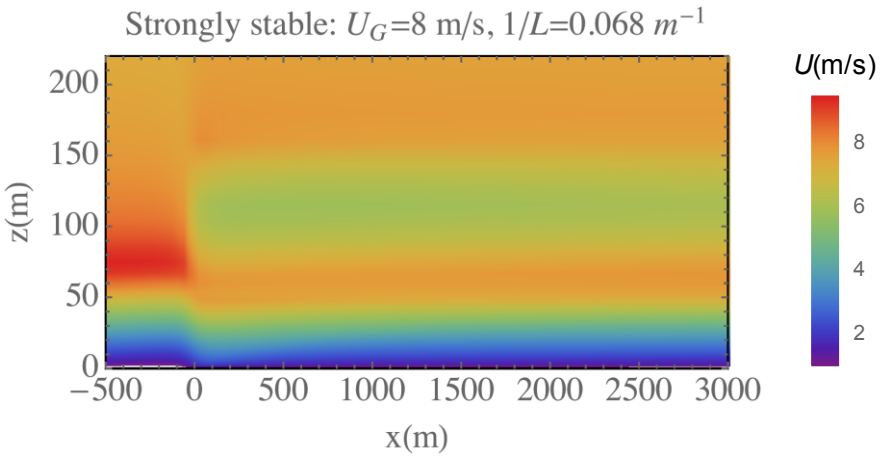

Figure 4-3. Flow field for most stable (rarest) simulated case.

Situations like the stable, shallow-ABL case shown in Figure 4-3 can lead to ducting and enhanced long-range propagation, or also increased attenuation, depending on the ABL depth and the terrain.

4.1.3 Propagation model

A spectral parabolic equation (PE) solver was used to calculate the propagation, with ScaDis velocity fields as boundary conditions. The PE solver calculates the frequency-dependent propagation, given a source spectrum; more details can be found in Balras *et al* (2016, 2017). The turbine noise source was modeled as a superposition of three effective (lumped) sources, located at 46, 80, and 114 m respectively; in this way, the height-distributed aspect of the acoustic source was approximated for two-dimensional simulation (e.g. the 80m height corresponds to mid-level, out-of-plane blade positions. For each flow field, per each frequency (band), three separate 2D simulations were carried out, one for each lumped source height; the results were subsequently superposed, to give the expected mean acoustic field for a given case. The bottom boundary condition for the PE solver was a flat grass surface with associated acoustic impedance, and the acoustic propagation calculations were done for one-third octave bands up to 1 kHz, with source level $LW(f)$ as shown in Figure 4-4.

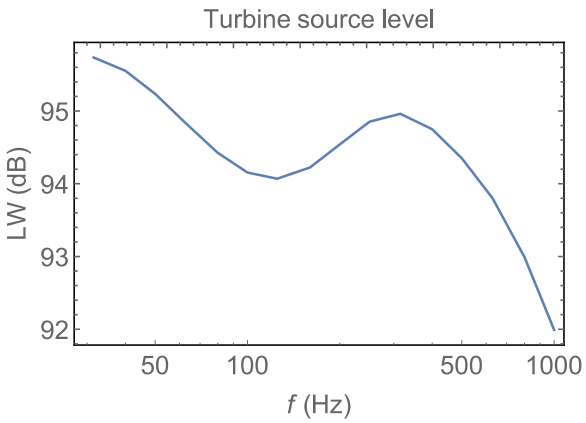

Figure 4-4. Effective turbine noise source level.

The total propagation result per frequency f for distance r downwind from the source is found via

$$\mathrm{SPL}(f) = \mathrm{LW}(f) - 10\ln(4\pi r^2) - \alpha(f)r + \Delta L(f) \qquad (4.2)$$

where the terms on the right-hand side are the source power level, geometrical spreading, atmospheric absorption, and finally the transmission loss calculated from the PE.

4.2 Main results

The sound pressure levels found via the PE propagation code and (4.2) are shown in Figure 4-5 for all cases considered, at height 2 m above ground.

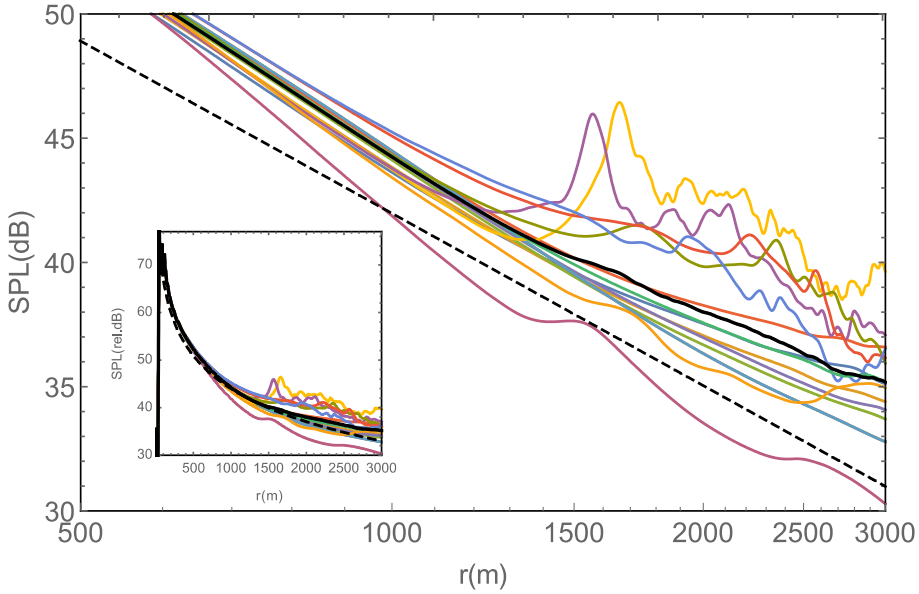

Figure 4-5. Total SPL for all cases (colored lines). Solid black line is probability-weighted mean; dashed line is -10log(r/100m) reference slope. Inset: same plot, with linear *r*-axis.

In addition to the different stability cases (colored lines), Figure 4-5 shows the total result (solid black line) calculated using all the cases with the probabilistic model (eqn. 4.1) using the Lille Valby values for the stability distribution (corresponding to Figure 4-1). For reference, the figure also displays a dashed line going as $10\ln(1/r)$, which is effectively cylindrical spreading.

The stable cases contribute most to elevating the sound pressure level at longer distances, due to (wake-affected) refraction. Figure 4-6 shows the stable cases together, indicating the stability for each case; in addition to the total weighted mean (solid black as in Figure 4-5), the figure al-

so displays the weighted mean SPL for the stable cases only (dotted black).

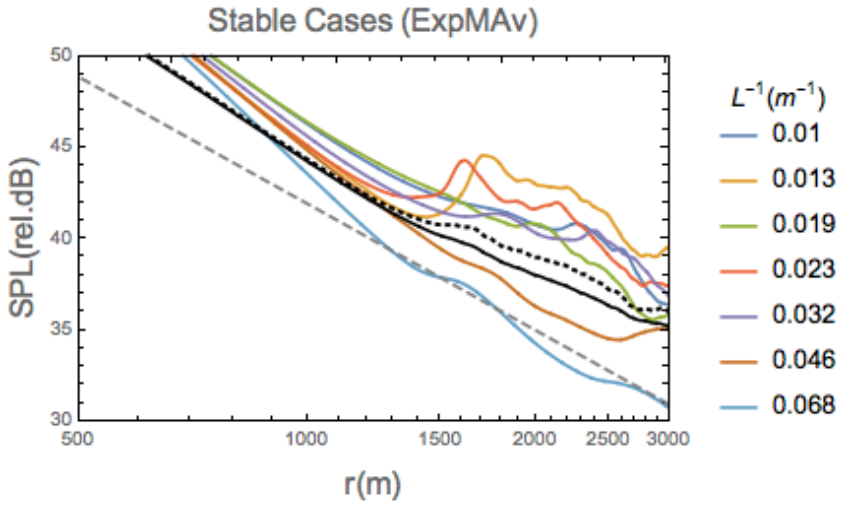

Figure 4-6. Total SPL for stable cases, plus probability-weighted mean for all (solid black) and for all stable (dotted black) cases.

From Figure 4-6 one can see that the most stable cases lead to more sound reduction, due to the shallow ABL depth accompanying them in the modeled flow field. Cases with modest stability, which are accompanied by ABL depths greater than twice the rotor top height ($h > 2z_{top}$) in the RANS simulations, show the loudest levels at long distances. Alternately, as mentioned earlier, from the light-blue and brown lines (L^{-1} of 0.046 and 0.068 m^{-1}) one sees that the most stable cases, with ABL depths and associated jets occurring below rotor top (as in Figure 4-3), give the lowest sound levels.

In the analysis and results thus far, we have not included the effects of the temperature profile. Although ScaDis provides $T(z)$, it was not used in the sound speed profile $c(z)$ for the PE solver, because the wind speed and shear contribute much more to $c(z)$. But for very stable cases with a shallow ABL, the temperature might have a significant effect. Indeed, incorporating the temperature profile into $c(z)$ changes the results for such cases, as depicted in Figure 4-7. The figure compares results with and without the effect of $T(z)$, for both the longest-propagating case (a weakly stable case with the highest wind speed) and the most stable, lowest-noise case; the other stable case results without $T(z)$ are shown in gray. One can see in the figure that the weakly-stable, lowest transmission loss case (red versus orange lines) is not affected much by inclusion of the temperature profile; however, the most stable case (blue versus teal lines) is significantly impacted by accounting for $T(z)$ in $c(z)$, with an increase of several dB in SPL for distances beyond 1km. Thus inclusion of $T(z)$ for very stable cases increases the long-range SPL predictions, though the weighted mean does not change much because very stable cases occur very infrequently; further, the propagation in stable cases becomes no less effective than in unstable cases.

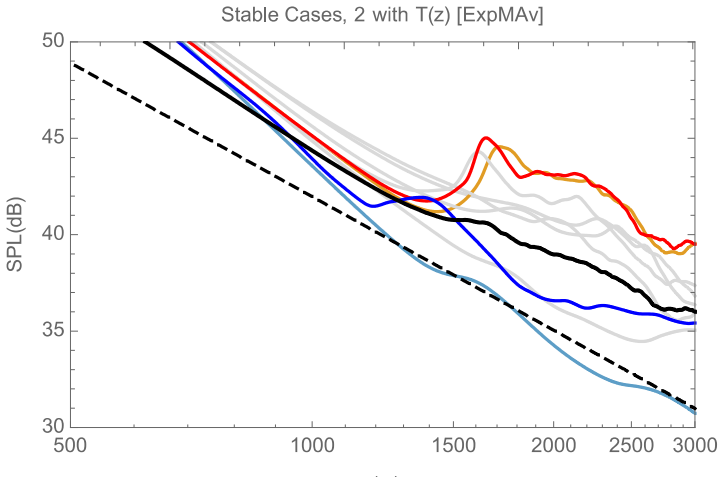

Figure 4-7. SPL without $T(z)$ as in Figure 4-6 (grey, teal, tan), plus results including $T(z)$ for two cases: a weakly stable case (red/tan with/without $T(z)$, $L^{-1} = 0.013\ \mathrm{m}^{-1}$) and strongly stable shallow-ABL case (blue/teal with/without $T(z)$, $L^{-1} = 0.068\ \mathrm{m}^{-1}$).

To further demonstrate the utility of the probabilistic method, as driven by a strategically sampled set of PE and RANS simulations, Figure 4-8 displays the total SPL for three representative climates, calculated using (4.1). The climates are: the typical (Lille Valby) case considered above, and the two site climates dominated most by stable (Cabauw, NL) and unstable (Basel, Switzerland) conditions, respectively, found by Kelly & Gryning (2010). The stability distribution $P(L^{-1})$ and consequent simulation-case weights a_i corresponding to each of these were found based on the measured $\{n_+, \sigma_+, \sigma_-\}$ from each site; then the weighted average of all cases was calculated for each site via (4.1).

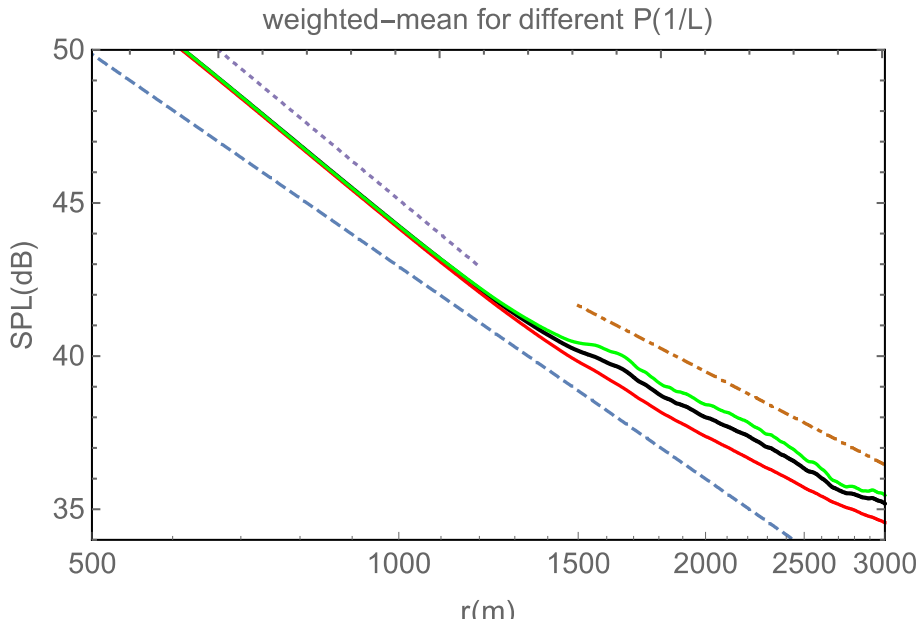

Figure 4-8. Overall weighted-mean SPL for different climates. Black: typical mid-latitude (Lille Valby, as in previous figures); green: more stable climate (Cabauw); red: more unstable climate (Basel). Dashed line is reference for cylindrical spreading; dotted line is $r^{6/5}$, dash-dot/brown is $r^{3/4}$.

From Figure 4-8 one can see that there does not overall appear to be a large difference in SPL, when stability-affected propagation results are in effect averaged according the frequency of conditions at each site: there is less than 1 dB difference between the stably-dominated Cabauw case and the unstable/convectively-dominated Basel site results, with the typical site of Lille Valby falling closer to the Cabauw site's results. This is not completely surprising, since neutral conditions dominate the stability distribution. But we note that the calculations presented in Figure 4-8 were done without the temperature profile; thus, as demonstrated with Figure 4-7, if we re-calculate all the cases including $T(z)$, then the SPL increases for the most stable cases, and we expect the green line in Figure 4-8 to move up away more from the 'typical' and local result signified by the black line. The figure also indicates that over distances up to 3km the propagation is roughly approximated by cylindrical spreading (dashed line), but more particularly with the SPL decaying a bit faster (as $r^{-6/5}$, dotted line) for medium distances out to ~1200m or ~$15 \times z_{hub}$ downwind, then decaying more slowly than cylindrical (ca. $r^{-3/4}$, dash-dot line) beyond ~$20 \times z_{hub}$.

4.3 Conclusions

We have created and implemented a probabilistic model for wind turbine noise propagation through the stability-affected atmosphere including the turbine wake, based on output from simulations using a parabolic-equation acoustic propagation model, which in turn is driven by flow-field outputs from an atmospheric RANS model. The effect of stability on the flow field, including the depth of the ABL and shear associated with such, as well as the stability-affected turbine wake, are modelled within the RANS model. This model-chain was applied to examine three cases, one of which corresponds to the field measurements at Risø.

We found a number of things from our investigation. First, contrary to simple intuition, the most stable conditions do not necessarily lead to the loudest sound levels in the far field. Rather, the depth of the ABL (relative to hub/rotor height) has an effect, and subsequently that *weakly, more commonly-occurring* stable conditions can lead to the highest sound levels for distances more than 1 km downwind. Thus simply picking a very stable and very unstable case (as in e.g. Barlas *et al.,* 2017) does not necessarily give an indication of the range of expected sound pressure levels. Associated with this is the verification that including the temperature profile (within the sound speed profile) has a bigger effect on the most stable conditions, increasing the SPL at long range. We do however note that the current results were done without modelling the scattering effect of turbulence, and that it is possible that for the more common, weakly stable cases—which showed the highest SPL at distance—the SPL may reduce a bit due to scattering, since turbulence is less effectively suppressed by buoyancy for more weakly stable conditions.

While probability-weighted conditional second-order moments are not given here, with our analysis we estimate that one can expect an SPL variability on the order of 5 dB for distances of 1-3 km (over simple terrain) during night-time, which is when noise perception is most crucial. Over a significant range of stable conditions, the current results indicate that turbine noise is still perceptible (e.g. SPL>35 dB) beyond 3km distance in the downwind direction.

Ongoing and needed work includes extending the calculation to 5km or more and also at angles to the wind (3-D), inclusion of the temperature *profile* effect on sound speed for all stability cas-

es, calculating conditional variances to determine nighttime variability and its dependence on the climatological stability parameters, as well as repeating the PE simulations including basic scattering and over different roughnesses.

References

Barlas E, Zhu WJ, Shen WZ, Andersen SJ (2016) Wind turbine noise propagation modelling: An unsteady approach. *Journal of Physics: Conference Series (online) – The Science of Making Torque from the Wind 2016,* **753** [022003] (11pp); doi 10.1088/1742-6596/753/2/022003.

Barlas E, Zhu WJ, Shen WZ, Kelly M (2017) Effect of Wind Turbine Wake on Atmospheric Sound Propagation. *Applied Acoustics*, under review (s.4/2016).

Kelly M & Gryning S-E. (2010). Long-Term Mean Wind Profiles Based on Similarity Theory. *Boundary-Layer Meteorology*, **136**(3), 377-390.

Kelly M & Troen I (2016). Probabilistic stability and "tall" wind profiles: theory and method for use in wind resource assessment. *Wind Energy*, **19**(2), 227–241.

Sogachev A, Menzhulin G, Heimann M, Lloyd J (2002) A simple three dimensional canopy—planetary boundary layer simulation model for scalar concentrations and fluxes. *Tellus* **54**B:784–819.

Sogachev A, Kelly M, & Leclerc MY (2012). Consistent Two-Equation Closure Modelling for Atmospheric Research: Buoyancy and Vegetation Implementations. *Boundary-Layer Meteorology*, **145**(2), 307-327.

5. WP.3-B: Coupling of Noise Source and Propagation Models

WP Manager: Mark Kelly
Participants: Emre Barlas, Wei Jun Zhu, Wen Zhong Shen

Objectives

The main objective of WP.3B is to develop a reliable noise generation and propagation coupling strategy that can predict correctly and accurately noise generated from wind turbines at a long/large distance from the turbines. The coupling needs the detailed information about the noise characteristics at the turbines and makes the use of the information to the noise propagation model.

5.1 Introduction

Sound pressure levels at far field receivers are largely influenced by the source characteristics at the turbines as well as the medium between the turbines and the receivers in which the sound propagation takes place. In order to address this issue, an advanced unsteady coupling approach has been developed in CCA-WTN2016 using a source model such as the BPM semi-empirical wind turbine noise generation model, a propagation model based on solving the parabolic wave equation (PE), and a flow model based on solving the incompressible Navier-Stokes equations with Large Eddy Simulation.

5.2 Computational models

For this study the three-bladed, stall regulated Nordtank NTK 500/37 wind turbine with a 500 kW nominal power is used. The hub height is 35 m and the rotor diameter is 41 m. For further technical details about the turbine, the reader is referred to [1]. The employed noise source, noise propagation and flow models are first presented in the next three subsections, followed by the fourth subsection, which describes the coupling technique.

5.2.1 Wind turbine noise source model

In this CCA-WTN2016 project, we use the recent noise generation model developed at DTU which integrates NREL's NAFNoise (NREL AirFoil Noise) code [2] with NREL's FAST8 (fatigue, aerodynamics, structures and turbulence) modular framework [3]. This integration allows modeling aerodynamic noise generated by the blades with the consideration of the wind turbine structural dynamics and its interaction with the incoming turbulent flow. As the way used in the blade element theory, each blade is divided into a number of two dimensional airfoil elements. The total noise level at a given receiver location is predicted as the sum of the contributions from all blade elements. In the present study, only two types of aerodynamic noise sources have been included, namely the trailing-edge noise and the turbulent inflow noise. The used models and the methods for obtaining the necessary inputs are explained below.

Trailing-edge noise

The total sound pressure level of noise generated from the interaction of the turbulent boundary layer with the trailing edge is calculated through the summation of the different contributions of noise on the pressure side, on suction side, and from flow separation. These three noise mechanisms can be modelled semi-empirically using scaling laws (see Brooks, Pope, and Marcolini (BPM) for more details). Different to the classical BPM noise generation model, the boundary layer characteristics in this study are obtained from Q^3UIC (DTU's integral boundary layer solver) which is shown to predict the boundary layer characteristics more accurately than XFOIL [4]. Additionally, a conditional switch used in the classical BPM model to turn on the separation noise is the angle of attack flag, which was set to be 12.5 degrees. The value is modified according to the lift coefficient curves of the airfoils used in the blade.

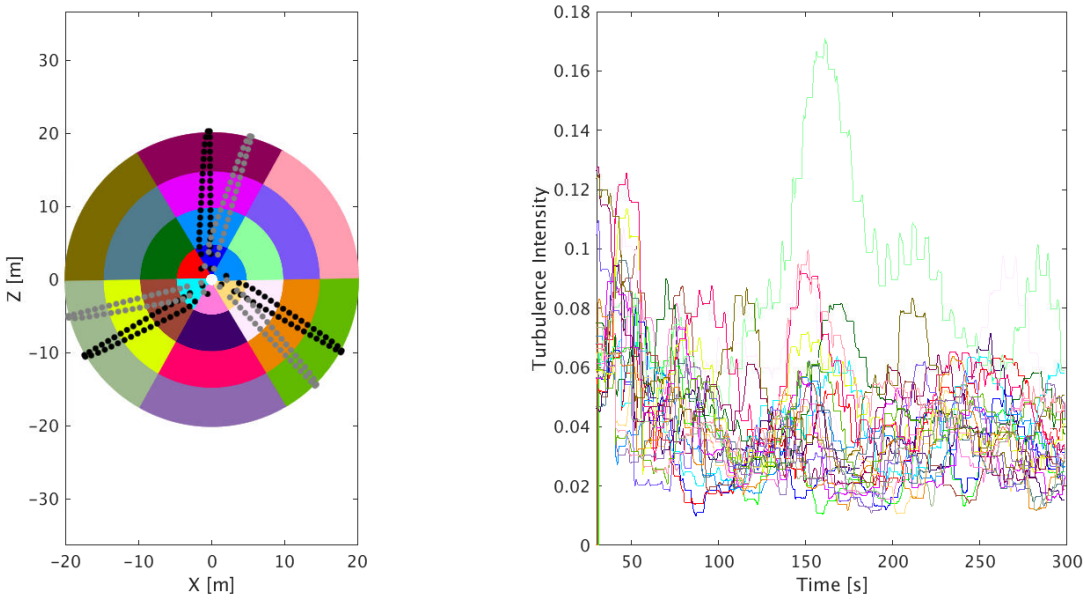

Figure 5.1: Left: Colored 24 regions of the rotor swept area for turbulence intensity calculations. Right: Time-dependent turbulence intensity signals in the 24 regions, marked with the same colors as for the regions.

Turbulent inflow noise

The turbulent inflow noise model originally proposed by Amiet [5] and further developed by Lowson [6] is used for inflow noise estimation. Additionally the correction for airfoil thickness proposed by Moriarty and Guidati [7] is applied. The turbulence intensity (TI) is calculated by taking into account the inflow characteristics obtained from LES simulations (Section 5.2.3) and instantaneous airfoil locations. The rotor area is divided into 24 regions obtained with azimuthally 6 and radially 4 divisions. As the blades rotate, in each region, the wind speed is sampled, and the standard deviation and local mean value are calculated. The sampling time-duration is chosen to be 5 seconds that corresponds to 500 samples. Afterwards the TI value in each region is updated according to the actual standard deviation and average (see Figure 5.1). At each time-instant the TI value in the region where an airfoil is located is assigned to the airfoil. Additionally, a turbulent length scale is calculated using the relationship in [8] that can be expressed as a function of surface roughness zo and height z: $\mathrm{L} = 25 * \mathrm{z}^{0.35} * \mathrm{z}_0^{-0.063}$.

5.2.2 Sound propagation model

For modelling the sound propagation, the in-house Parabolic Equation (PE) based sound propagation tool WindSTAR-Pro (Wind turbine Simulation Tool for AeRodynamic noise Propagation) is used. The tool implements the two-dimensional Generalized Terrain PE method [9] in FORTRAN environment with the MPI parallelization strategy in frequency and realization/time step. The PE method is a solution of the parabolic wave equation for harmonic waves in forward propagation with a finite angle. The conventional PE method uses an effective sound speed approach where the moving atmosphere is modelled with a hypothetical motionless medium and an effective sound speed of $C_{eff}(x,z) = c(x,z) + V_x(x,z)$ where V_x is the wind velocity component along the direction of propagation between the source and the receiver, obtained from the flow solver described in the next section. In order to study the refraction phenomenon dominated by the wind speed deficit and its fluctuations around the wind turbine, the speed of sound is chosen to be constant ($c(x,z) = 340\frac{m}{s}$) in the computational domain. The spatial resolution in both directions of the 2D PE domain is set to be one-eighth of the wavelength ($\Delta x = \Delta z = \frac{\lambda}{8}$). The terrain is flat with a ground impedance characterized using the Delany-Bazley model [10] and an effective flow resistivity of 200 $kPa.s/m^2$, representing a grassland. All simulations are carried out for the 1/3- octave band center frequencies up to 2000 Hz and then summed logarithmically to obtain an overall SPL as follows:

$$L_{p_{sum}} = 10\log_{10}\sum_{i=1:N} 10^{Lp(f_i)} \quad (5.1)$$

where N is the number of considered frequencies and $L_p(f_i)$ is the sound pressure level at frequency f_i defined as:

$$L_p(f_i) = L_W(f_i) - 10\log_{10} 4\pi r^2 - \alpha r + \Delta L \quad (5.2)$$

The source power level of a wind turbine ($L_W(f_i)$) is obtained from the source model described in the previous subsection, the second term on the right hand side stands for a geometrical spreading, the third term represents an atmospheric absorption with an absorption coefficient defined in ISO 9613-1 for air at 20°C with 80% relative humidity. The last term is the relative sound pressure level $\Delta L = 20\log_{10}(p'/p_f)$ that represents the deviation from the free field sound source due to the ground effect, atmospheric refraction, turbulence etc. This last term is obtained from the noise propagation method.

5.2.3 Flow model

The in-house pseudo-spectral 3D Navier-Stokes solver is used, which implements the Smagorinsky subgrid scale model for large eddy simulation (LES) [11]. First, a precursor simulation is run to establish the developed boundary layer on a ground surface with a surface roughness of 0.2. This solution is then fed into the computational domain with the wind turbine. The wind turbine rotor is modelled via the actuator line technique, in which the body force is distributed radially along each rotor blade. The domain of [1500 m X 400 m X 400 m] is discretized with a resolution of [600 X 160 X 320] in the streamwise, lateral and vertical directions, respectively. The time step is chosen to be 0.07second, while sampling time for the propagation simulations were 0.1 second.

5.2.4 Coupling procedure

Figure 5.2 depicts the coupling procedure with 6 steps listed below:

- First, the flow field is simulated using LES (see Section 5.2.3 for the flow model). At each time step a two-dimensional (Y-Z) slice at 2D upstream of the wind turbine as well as the whole three-dimensional field are stored.

- This flow field is used as an input to FAST8. Thereby a fully aero-elastic turbine is exposed to a realistic atmospheric flow.
- Frequency dependent sound pressure levels at given receiver locations are calculated and stored via the integrated aeroacoustics module in FAST8 (see Section 5.2.1 - source model). 25 receiver locations are chosen and shown in Figure 5.2.
- At these receiver locations, in addition to the sound pressure levels, the highest SPL contributions at each time step for each frequency and each blade are detected and their coordinates are stored.
- A two-dimensional PE domain (see Section 5.2.2 – propagation model) is constructed between each blade and each receiver in considering the detected source locations.
- At each time step, two-dimensional PE simulations are carried out for 3 blades, 20 frequencies and 25 receivers (in total 1500).

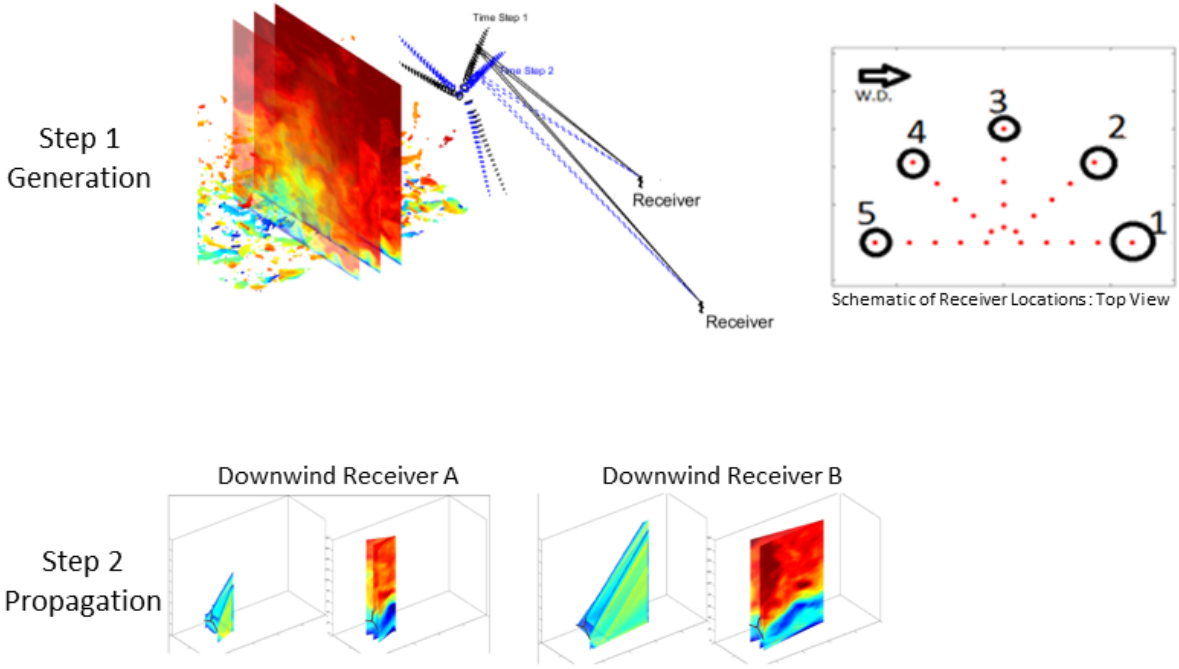

Figure 5.2: Overview of the coupling steps. Step 1: Noise generation via FAST8+NAFNoise. Step 2: Propagation via 2D PE simulations from each blade to selected receivers. The procedure is repeated at each time-step.

5.3 Main results

Three sets of simulations are carried out that are described below:

- Only source simulations ($\mathbf{SPL_S}$): Output of FAST8+NAFNoise at various receiver locations. This means that the last two terms in Equation (5.2) are neglected, e.g. the atmospheric absorption, and the ground reflection and refraction due to atmosphere.
- Propagation over a grassland ($\mathbf{SPL_{S+P_G}}$): Coupled source and propagation simulations for which the ground impedance value is representative for a grassland and the full three dimensional flow field is taken into account as explained in Section 5.2.4.

- Propagation over a hard ground ($\mathbf{SPL_{S+P_{HG}}}$): Coupled source and propagation simulations for which the ground impedance value is infinity for a fully reflective hard ground and the fully three-dimensional flow field is taken into account as explained in Section 5.2.4.

In order to investigate the effect of propagation at various receiver locations, the focus is on the differences of SPL values, namely ΔSPL;

$$\Delta_{\mathrm{SPL\ G}} = \mathrm{SPL}_{\mathrm{S+P_G}} - \mathrm{SPL_S} \quad \text{and} \quad \Delta_{\mathrm{SPL\ HG}} = \mathrm{SPL}_{\mathrm{S+P_{HG}}} - \mathrm{SPL_S}$$

5.3.1 Time averaged SPL

Figure 5.3 shows the time averaged Δ_{SPL} for multiple receivers at 2 m height. The plot in the upper half domain is the solution for the grassland and the plot in the lower half domain is the solution for the hard ground. Thereby the effect of ground impedance is also investigated. The first observation can be deducted from Fig. 5.3 is that both $\Delta_{\mathrm{SPL\ G}}$ and $\Delta_{\mathrm{SPL\ HG}}$ are negative in the upwind area at a certain distance from the turbine. This is expected as the sound waves are refracted upwards due to the wind. Nevertheless positive values are observed in the upwind region at 220 m for the grassland, while the distance is 320 m for the hard ground. This is due to the different ground impedance values that cause constructive and destructive interference between direct and reflected waves at different locations. While the grass ground absorbs some of the oncoming waves, the hard ground is fully reflective. A similar trend is observed in the crosswind direction. However, the distances are different. The increased distances due to propagation effects are 200 m and 600 m for the grassland and hard ground, respectively. In the downwind direction, it is seen that the propagation effects can cause a SPL increase at a distance up to 200 m for the grassland and up to 800 m for the hard ground.

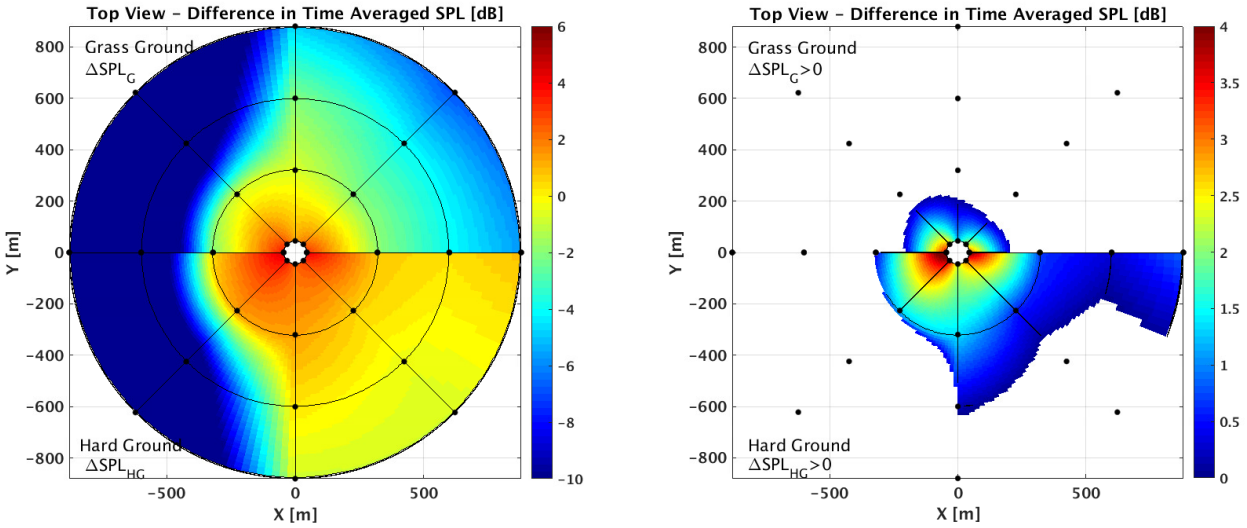

Figure 5.3: Left: SPL difference for a grassland and a hard ground ($\Delta SPL_G = SPL_{S+P_G} - SPL_S$ and $\Delta SPL_{HG} = SPL_{S+P_{HG}} - SPL_S$). Right: Plot of the positive SPL difference.

5.3.2 Time dependent SPL

As the new coupling technique is unsteady, we can investigate the time dependent SPL and look into the amplitude modulation. Figure 5.4 shows spectrograms for a receiver at 2 m height

and 45 m downwind of the turbine. The differential spectrogram ($\Delta_{\mathrm{SPL\,G}} = \mathrm{SPL}_{\mathrm{S+P_G}} - \mathrm{SPL}_{\mathrm{S}}$) gives some insight in the propagation caused fluctuations. Thereby the instances when the propagation effects cause an increase at far field are investigated for all receivers.

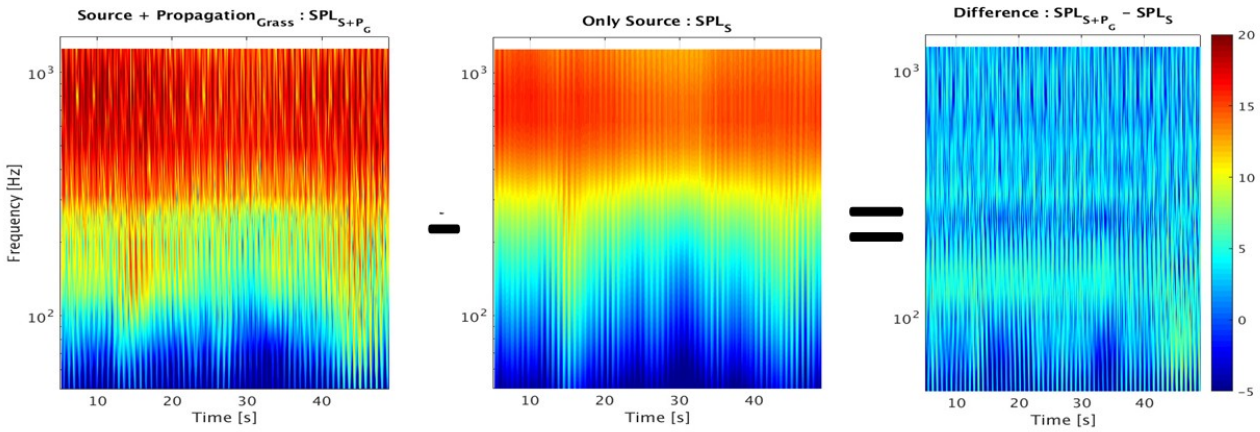

Figure 5.4: Spectrograms of sound pressure level for Source + Grass propagation (left), Only Source (mid) and Difference (right).

Some further observations can be deduced (due to the limited length of the report, the plots are not shown here) as follows:

- At 320 m, the downwind locations (receiver 1 and 2, see Fig. 5.2) have a clear trend of increased levels in the 300-500 Hz band for the hard ground and in the 300-400 Hz band for the grassland.
- Crosswind simulations (receiver 3) show increased levels at distances of 320, 600 and 800m for the frequencies less than 300 Hz. This increase for frequencies in this frequency band is not fully clear yet however it is observed that these levels are much higher for the hard ground.
- Upwind simulations show (receiver 4 and 5) that there are increased levels at 45 m and 320 m, and the propagation included simulations have a much lower SPL.

5.4 Conclusion and future work

In this CCA task, a new coupling technique has been developed that couples the wind turbine noise generation and propagation models simultaneously. Further detailed investigations will be conducted for the quantification of amplitude modulation in order to detect and possibly mitigate the far field AM levels.

5.5 References

[1] S Markkilde Petersen, Wind turbine test NORDTANK NTK 500/37 system test, Annual report year: 1994, Risø National Laboratory for Sustainable Energy, Technical University of Denmark.
[2] P Moriarty, NAFNoise, User's Guide (National Wind Technology Center, National Renewable Energy Laboratory, USA, Golden, Colorado, 2005).
[3] J Jonkman, The New Modularization Framework for the FAST Wind Turbine CAE Tool, NREL/CP-5000-57228, January 2013.
[4] NR García, JN Sørensen, WZ Shen, A strong viscous–inviscid interaction model for rotating airfoils, Wind Energy Volume 17, Issue 12, December 2014 , Pages 1957–1984.
[5] RK Amiet, Acoustic radiation from an airfoil in a turbulent stream, Journal of Sound and Vibration, vol. 41, pp. 407-420, 8/22/1975.

[6] MV Lowson, (1993), Assessment and prediction of wind turbine noise, Flow Solutions Ltd., Bristol.
[7] PJ Moriarty, G Gianfranco, P Migliore (2005), Prediction of Turbulent Inflow and Trailing-Edge Noise for Wind Turbines, 11th AIAA/CEAS Aeroacoustics Conference Monterey, California.
[8] J Couniham, 1975, Adiabatic Atmospheric Boundary Layer: A Reviewed and Analysis of Data from the Period 1880-1972, Atmos. Environ., 9, pp.871–905.
[9] RA Sack and M West, A Parabolic Equation for Sound Propagation in Two Dimensions over Any Smooth Terrain Profile, 1994, Applied Acoustics.
[10] ME Delany and EN Bazley, Acoustical properties of fibrous absorbent materials, Applied Acoustics 3, 105-116, 1970.
[11] OD Kaya, Development of Large Eddy Simulation Tools for Simulation of Atmospheric Boundary Layers in Wind Farms, PhD Thesis,

6. WP.4: Development of Wireless Microphones for Sound Propagation Measurements

WP Manager: Torben Mikkelsen
Participants: Steen Sørensen, Per Hansen, Franck Bertagnolio, Stuart Bradley (University of Auckland, NZ), Michael Kerscher (Gfai Tech, Berlin).

Objectives

The WP4 project objectives were to further develop the set of 42 wirelesses Wi-Fi mic's and make test measurements with them in 2016.

Figure 9 - Steen Sørensen DTU/TEM in the test field next to one of the 42 wireless mics during testing at Campus Risø in November 2016. On the plate is seen: One mic with B&K wind sock connected to a Nokia mobile telephone and a battery package. This autonomous WIFI network connected mic system. With the battery package shown each of the autonomous GSM network controlled mic systems is able to record and transmit time series of noise measurements continuously for a 12 hour period.

Main results concerning Wireless Wi-Fi Mics (42)

In 2016 we have tested and begun to calibrate the microphones.

We experienced some difficulties with the Nokia telephones automatic gain control (AGC) that resulted in we needed to attenuate the mics preamplifiers output voltage to be less than 1 mV to avoid uncontrolled automatic gain control of the in the Nokia devise.

Two test measurements have been conducted in 2016; see attached SLP measurements compared to a standard ref mic (type BSWA Technology).

Figure 10 - The position of three wireless mics during test measurements around the Nordtank test turbine during the summer of 2016. Three test positions around the test turbine were chosen: A - equipped with BSWA Mic no. 1 and Wi-Fi mic A; B equipped with BSWA Mic no. 5 and Wi-Fi Mic B, and C equipped with BSWA Mic no. 4

Each measurement position was equipped with both a BSWA Technology reference mic and a WIFI test mic. The panel below shows measurements with the Nordtank running, and without the Nordtank turbine operating:

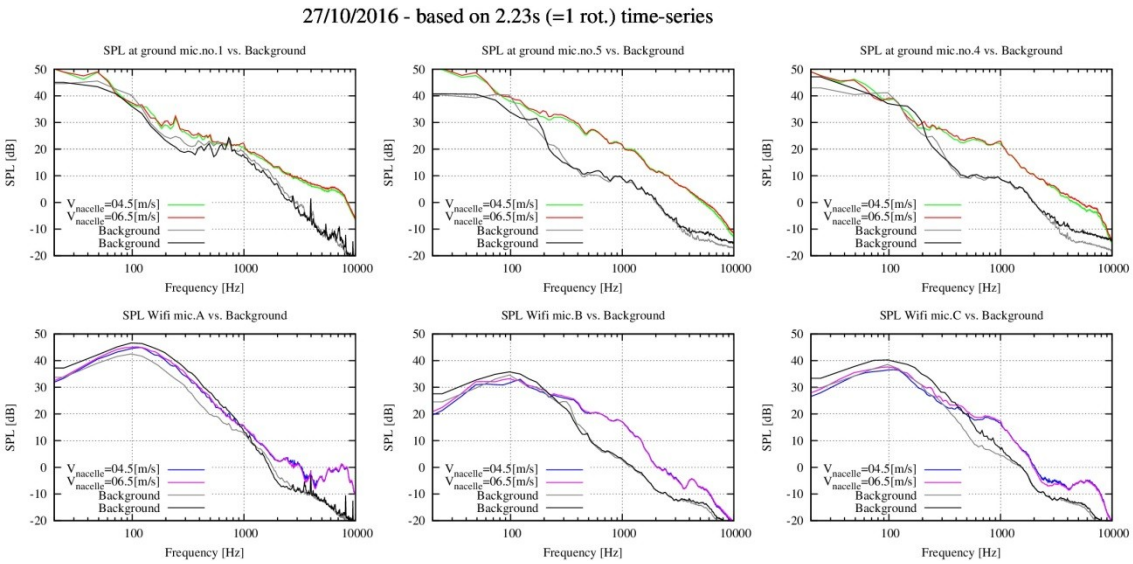

Figure 11 - Comparison between measured noise spectra at position A; B and C and at two different wind speeds 4.5 m/s and 6.5 m/s. Upper panel: Noise spectral measurements from the grass reference mics.. Lower panel: Spectral measurements with the co-located Wi-FI mics.

Outstanding issues end 2016:

1. We still need to make/manufacture 42 attenuation connecting probes, one to each of the 42 mics, to mitigate the experienced AGC issues, before the 42 mics become fully operational for deployment.
2. We also still need to go to DTU's anechoic chamber at DTU Electro at campus Lyngby to record detailed spectra reference measurements for spectral calibration in the frequency range where the mics are applicable, that is from 100 Hz to a few k Hz. Frequencies below 100 Hz, say down to 50 Hz will be useful following a post calibration of the measured spectra in the interval 50 Hz to 100 Hz, but the wireless mics are not designed for infra-sound measurements.
3. The test measurements showed a roll-off at around 100 Hz compared to the reference microphones. This could be caused by the amplifier and/or the microphone capsules.

Conclusion regarding the field testing with three Wi-Fi Mics in 2016:
From the field test in July it was concluded that the wireless microphones were too far away from the NordTank to capture anything significant noise above the threshold, but the test succeeded in the sense that the wireless system recorded for an extensive period of time without interruptions.

Main results concerning Acoustic camera sound measurements

Field measurements on the NordTank in November in collaboration with GFai and DTU Velux fund visiting professor Stuart Bradley.

Figure 12 - The FlexStar 120 mic acoustic antenna of 4 m diameter developed and deployed at Risø campus by GFai Berlin simultaneously with test activities with wireless mics at DTU Campus Risø, Nov. 2016.

In November 2016 GFai Tech (German acoustic camera manufacturer) and Stuart Bradley (University of Auckland) re- visited DTU-Risø Campus and together with DTU Wind energy performed noise measurement tests on the Nordtank 500/41 turbine. DTU Wind energy again placed three wireless mics in the surroundings around the test turbine for reference measurements. See the lay-out in fig.5 Prior to the testing a number of battery driven noise sources was attached to one of the blades, two facing backward and 6 facing forward

Noise measurements were conducted in the near-field using an acoustic camera brought by GFai Tech.

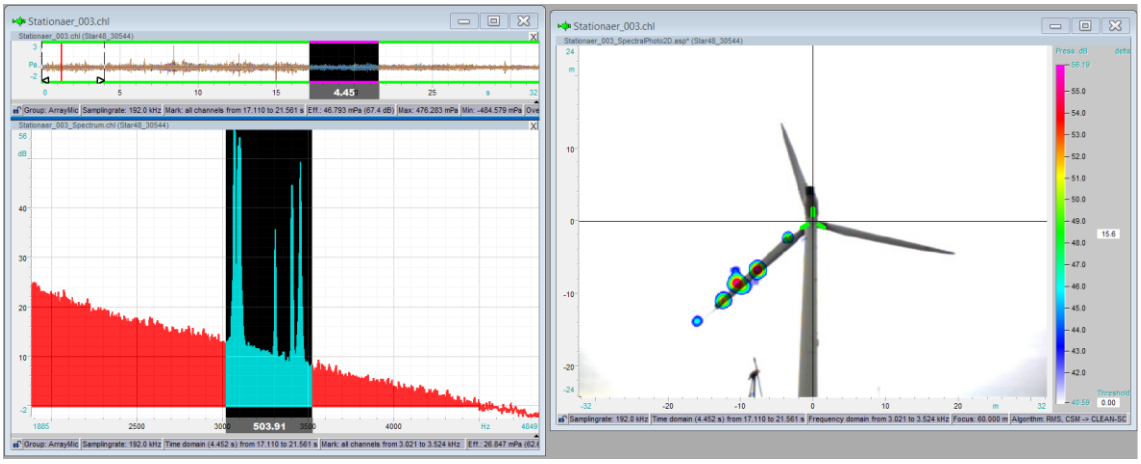

Figure 13 - Instant noise picture measured by the GFai acoustic camera of the Nordtank turbine at stand-still equipped with 6 discrete 3 kHz noise sources, six on the pressure side and two noise sources on the suction side on blade #1.

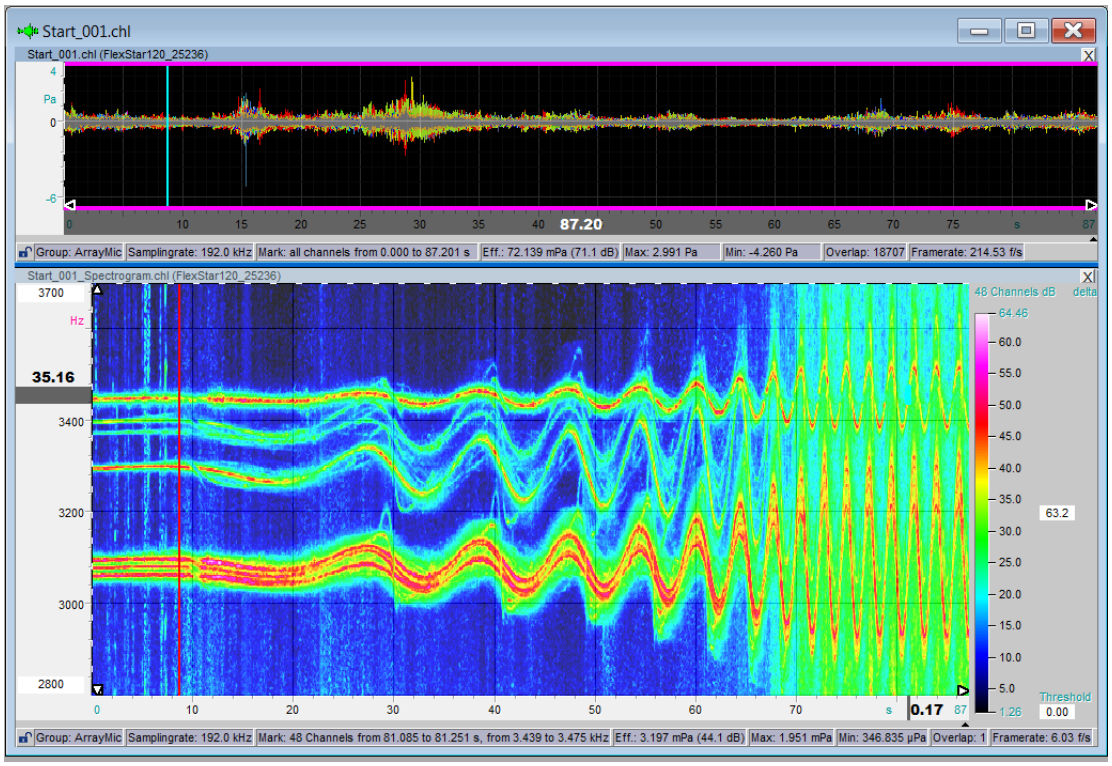

Figure 14 - Spectral measurements obtained with the FlexStar acoustic camera in front of the Nordtank turbine during Start-up.

A spectrogram of 80 s duration is shown in Fig. 5.6. The turbine blade mounted noise sources emit constant frequency sound in the frequency range just above 3 kHz but at slightly different discrete frequencies in the range between 3050 Hz to 3516 Hz. The upper panel shows the measured tine series in microphone no. 1 of the Gfai FlexStar set of 120 microphones. The other 119 microphones recorded similar data with high phase resolution, from which the acoustic pictures of the noise sources can be calculated. The lower panel shows the corresponding spectrogram during a 80 s period where the NordTank turbine starts up. The Doppler Effect is

clearly seen. In addition, as the turbine starts to rotate, additional noise to what comes from the sound sources is seen to be generated (the shadows at higher and lover frequencies generated beyond the frequency range of the noise source transmitted sound.)

The acoustic antenna data together with the Wi-Fi mic data are now being processed for analysis and the joint field experiment will be published in 2017.

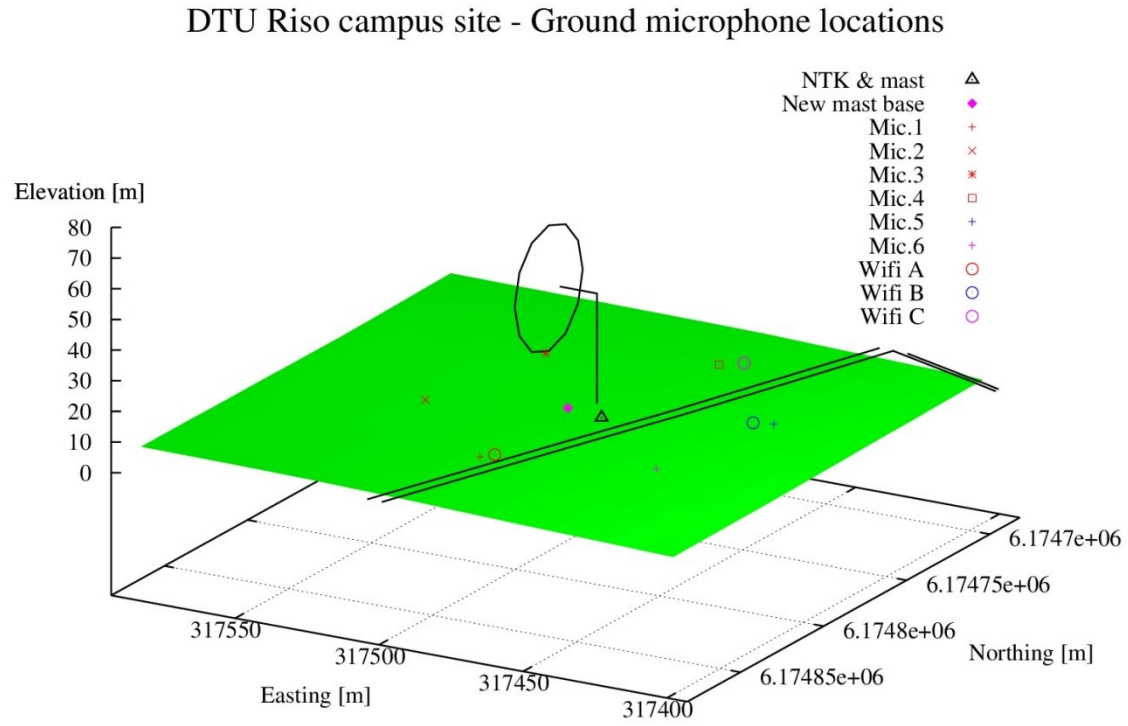

Figure 15 - Experimental layout of WI-FI and reference microphones around the DTU Nordtank turbine summer 2016.

Conclusions

The set of DTU Wind energy developed set of 42 autonomous operated wireless Wi-Fi mics are now close to a state where they are tested and soon calibrated, so they can be deployed in field tests in 2017.

The software on the phones has been improved. There was a problem when starting a measurement with more than one phone. The problem is now solved, and the software is quite stable and works as expected, even under extreme conditions.

Conclusions and Perspectives

In view of the results obtained and summarized in this report, many of the objectives set for this Cross-Cutting Activities on Wind Turbine Noise were reached. However, within each work package, further progresses still remained to be accomplished in order to achieve the ultimate goal of such study: the understanding of the whole chain of events occurring during wind turbine noise generation and propagation.

Concerning WP1, the autonomous system for flow monitoring on the blade (Pitot tube) have been further developed. More work needs to be done to make it fully autonomous (WIFI and energy supply) for longer periods of time. This work will be continued within one of the CCA 2017. Furthermore, an accurate calibration of the Pitot tube is still needed. The use of higher-frequency sampling is also considered in the future. The surface pressure microphone technology mounted on the blades is well understood. However, reliability of the GRAS microphones is still questionable. This will also be further investigated in the CCA 2017.

Two noise mitigation devices were tested on the Nordtank turbine and change in noise emissions could be detected. As part of the CCA 2017, it is intended to investigate the influence of the wind turbine controller of the V52 turbine on noise.

Progresses have been achieved in the understanding of noise propagation using statistical methods for atmospheric physics, and code development of advanced noise propagation methods using Parabolic Equations has also been advanced. However, much need to be done to fully understand the complex and interacting phenomena at play when noise is generated on the blades to its immission at a residential area.

Finally, an autonomous WIFI noise recording system using off-the-shelf mobile phones able to cover large terrain surface area in order to map wind turbine noise has been further developed and tested. The main challenge is now to improve the noise measurement accuracy so that this system compares satisfactorily with standard wind turbine noise recording systems using microphones connected by cables to a standard acquisition system. This last step will require: 1) probably new more accurate microphones to be connected to the mobiles phones, and 2) a calibration of the overall system in controlled conditions, e.g. in an anechoic chamber.

Bilag A - Project GANTT Chart and Deliverables

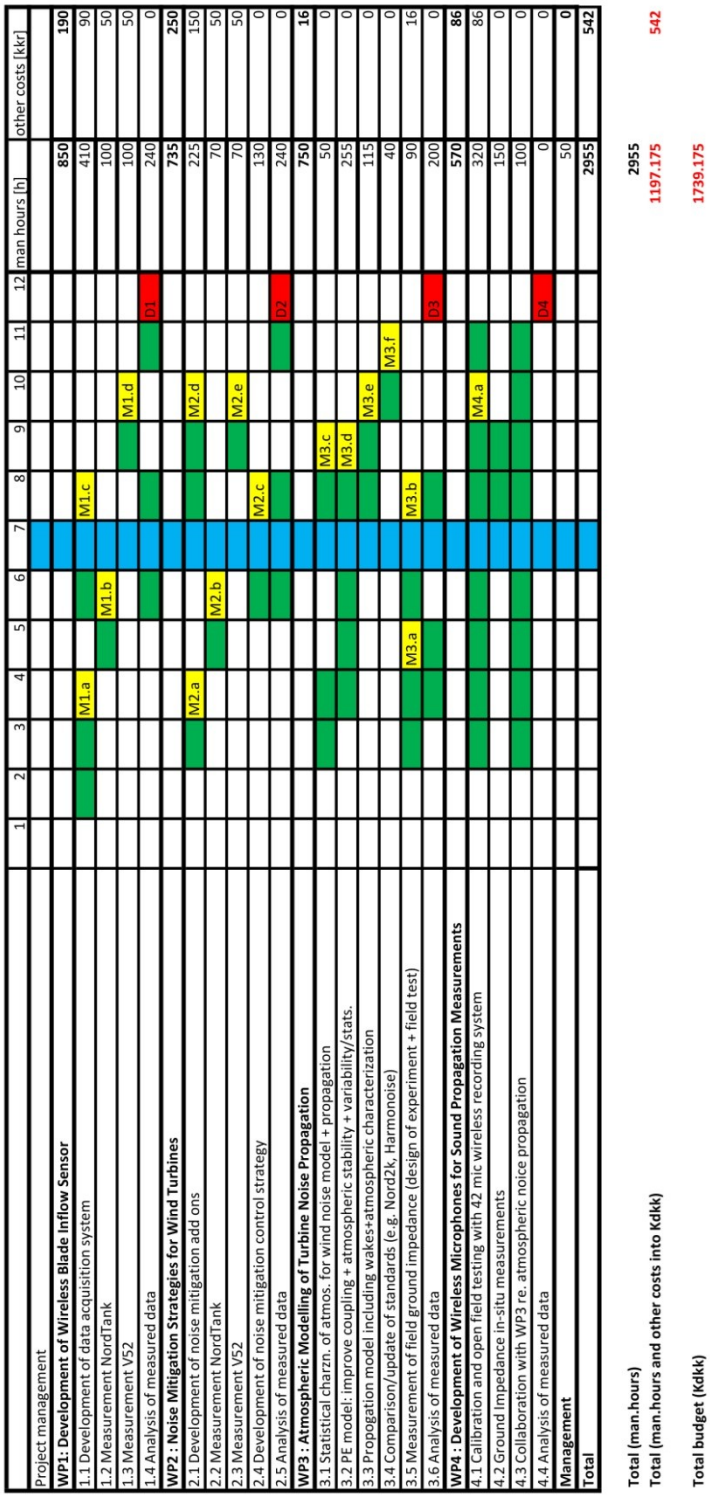

	1	2	3	4	5	6	7	8	9	10	11	12	man hours [h]	other costs [kkr]
Project management														
WP1: Development of Wireless Blade Inflow Sensor													850	190
1.1 Development of data acquisition system			M1.a					M1.c					410	90
1.2 Measurement NordTank					M1.b								100	50
1.3 Measurement V52										M1.d			100	50
1.4 Analysis of measured data												D1	240	0
WP2 : Noise Mitigation Strategies for Wind Turbines													735	250
2.1 Development of noise mitigation add ons				M2.a						M2.d			225	150
2.2 Measurement NordTank						M2.b							70	50
2.3 Measurement V52										M2.e			70	50
2.4 Development of noise mitigation control strategy								M2.c					130	0
2.5 Analysis of measured data												D2	240	0
WP3 : Atmospheric Modelling of Turbine Noise Propagation													750	16
3.1 Statistical charzn. of atmos. for wind noise model + propagation									M3.c				50	0
3.2 PE model: improve coupling + atmospheric stability + variability/stats.									M3.d				255	0
3.3 Propogation model including wakes+atmospheric characterization										M3.e			115	0
3.4 Comparison/update of standards (e.g. Nord2k, Harmonoise)											M3.f		40	0
3.5 Measurement of field ground impedance (design of experiment + field test)					M3.a			M3.b					90	16
3.6 Analysis of measured data												D3	200	0
WP4 : Development of Wireless Microphones for Sound Propagation Measurements													570	86
4.1 Calibration and open field testing with 42 mic wireless recording system										M4.a			320	86
4.2 Ground impedance in-situ measurements													150	0
4.3 Collaboration with WP3 re. atmospheric noice propagation													100	0
4.4 Analysis of measured data												D4	0	0
Management													50	**0**
Total													**2955**	**542**

Total (man.hours)	**2955**	
Total (man.hours and other costs into Kdkk)	**1197.175**	**542**
Total budget (Kdkk)	**1739.175**	

Figure 16 - GANTT Chart and Overview of Hours and Other Costs

Deliverables	
autonomous working data acquisition system + report	D1
noise reduction device and control strategies evaluated + report	D2
noise propagation model coupled with various components and tested + report	D3
measurement of far-field noise from wind turbine with wireless system + report	D4
Milestones	
autonomous acquisition unit ready for use on wind turbine	M1.a
NordTank measurement campaign finished	M1.b
data acquisition system upgraded	M1.c
V52 measurement campaign finished	M1.d
noise mitigation prototypes ready for testing	M2.a
add-ons tested on Nordtank	M2.b
noise mitigation control strategies implemented	M2.c
noise mitigation device patented?	M2.d
noise mitigation control strategies tested	M2e
design of experiment of ground impedance meas.- calibration of loudspeaker	M3.a
field measurements of ground impedance completed	M3.b
propogation model with atmospheric stability, variability, stats.	M3.c
PE model devpt. finished	M3.d
propogation model including wakes+atmospheric characterization	M3.e
comparison/update of standards (e.g. Nord2k, Harmonoise) report	M3.f
First noise propagation cross correlation measurements analysed	M4.a

Figure 17 - Deliverables and Milestones

Bilag B - Finlet Design and Technology

“Finlets” have been established as an effective trailing edge noise control technique through an extensive series of experiments at Virginia Polytechnic Institute and State University. The technology has been inspired from owls – a bird well known for its silent flight. Three dominant features of an owl’s feather are responsible for its stunning silence in flight – a leading edge comb, trailing edge serrations and a velvety down over the surface of the wing. Lilley [4] posited that the velvety down, a network of tiny fibres rising out of the feather surface, could be a significant noise reducing feature. Clark *et al*[1] performed a systematic study of owl’s feathers and tried to mimic the velvety down using different canopies which resembled wedding veils. The canopies were placed over different rough surfaces and the roughness noise and surface pressure fluctuations were measured in a wall jet tunnel. The canopies were found to attenuate the roughness noise significantly. The unidirectional canopy as seen in figure 2, consisting of a large number of parallel fibres (see figure) oriented along the flow direction just above the roughness, was the most effective treatment that reduced the surface pressure fluctuations by 30 dB.

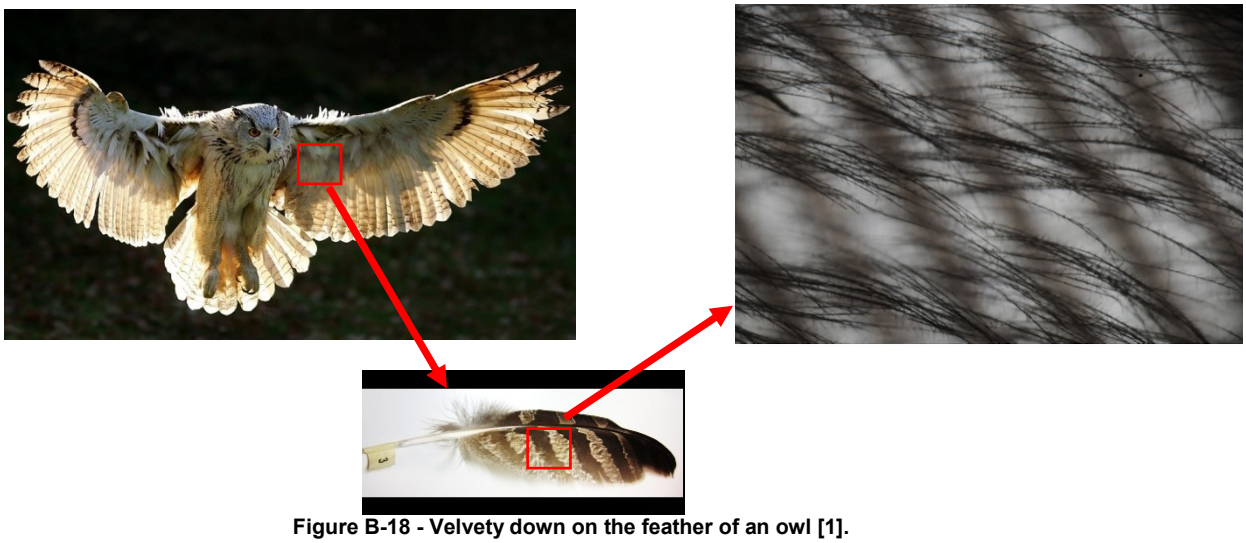

Figure B-18 - Velvety down on the feather of an owl [1].

The efforts were continued by Clark *et al* [2] where they developed and tested around 20 configurations of two surface treatments that replicated the effect of the unidirectional canopy in a form that was suitable for an application to an airfoil in external flow. These were called *finlet fences* and *rails*. Figure 3 below, demonstrates the finlets on a substrate that has been glued to the trailing edge region of the airfoil.

The treatments were applied directly upstream of the trailing edge to modify the boundary layer turbulence prior to the acoustic scattering by the trailing edge. The rear 12% (111 cm) of a 0.8 m chord tripped DU96-W180 research wind turbine airfoil was treated with these finlets on the pressure and suction side, and aeroacoustic measurements were performed at chord Reynolds numbers up to 3 million in the Virginia Tech Stability Wind Tunnel. Compared to the unmodified airfoil, the treatments were found to be effective, providing up to a 10 dB attenuation in the far-field trailing edge noise. The finlets were found to be effective over a wide range of angles of attack with minimal aerodynamic impact. Around twenty configurations with variations in the finlet

parameters shown in figure 4, were tested to understand the influence of the finlet geometry on the performance.

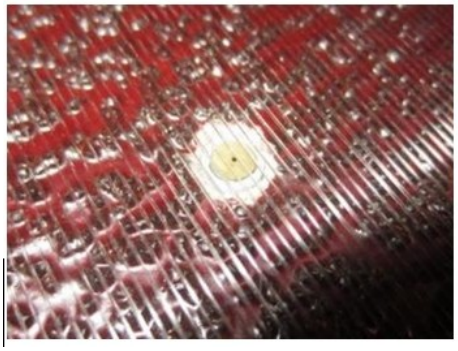

Figure B-19 - Unidirectional canopy from [2].

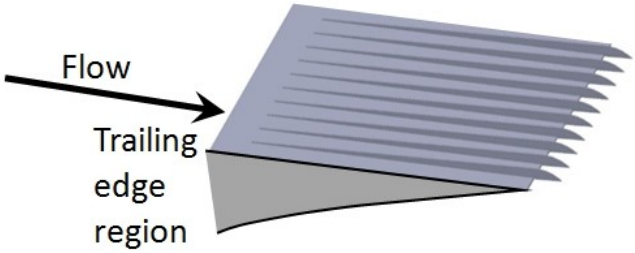

Figure B-20 - Demonstration of finlets [2].

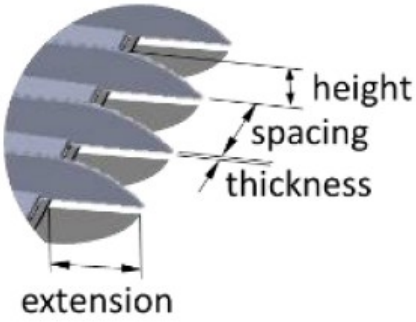

Figure B-21 - Finlet geometry parameters [2].

a) Finlet spacing and height

The finlets were found to be more effective when they were closely spaced. Four spacings of 1 mm, 4 mm, 6 mm and 10 mm were considered. This dependence appears consistent with the finlets limiting the spanwise correlation length scale – the smaller the spacing, the smaller the maximum correlation scale that can survive to the leading edge. However, below a certain spacing (between 1mm and 4 mm) the finlets behave as a single solid, much thicker blunt trailing edge, which manifests as an intense spike in the low frequency region of the trailing edge noise spectra as shown in Clark *et al* [2]. A spacing of 4 mm seemed to be the best choice of the considered spacings.

Doubling the fence height from 4 mm to 8 mm led to a reduction of 1 – 2 dB at almost all frequencies and angles of attack. This effect could be understood in terms of the boundary layer thickness at the trailing edge. Taller finlets would cut substantially more portions of the boundary layer, having a greater impact on the spanwise correlation length scale and thus the radiated noise.

b) Thickness and Extension

Extension of the finlets past the trailing edge was found to offer little benefit in terms of the noise reduction compared to the case without the extension, at lower angles of attack. The results were quite similar at higher angles of attack except that the high frequency noise levels (>3kHz) were lower without the extension. Clark *et al [2]* tested two thicknesses 0.5 mm and 2 mm and observed that thicker finlets were not detrimental to the acoustic performance of the treatment.

At frequencies above 1.5 kHz the thicker finlets caused a slight reduction (up to 3dB) in the noise levels. The results at lower frequencies were less clear. At lower angles of attack, the thicker finlets supressed the acoustic levels around 1100 Hz while the levels at 700 Hz were increased which were indicative of some organized turbulent motion at these frequencies due to the finlets.

Justification of the design

Based on the conclusions from Clark *et al* [2] and Clark *et al* [3], configuration (3) with a spacing of 4 mm, height of 8 mm, thickness of 0.5 mm (both the finlets and the substrate) and no extension beyond the trailing edge was found to be most effective. Hence the same configuration was considered for the field test. Similarly, 13% percent of the chord length beginning from the trailing edge was treated with finlets.

The blade geometry of the Nordtank wind turbine can be understood from the plots shown below. The variation in the chord is almost linear and gradual in the outer portion of the blade as indicated by the red line in the figures. A spanwise length of 5 metres beginning from 13.5 m radial distance to 18.5 m on both the pressure and suction sides was chosen for the treatment since the thickness and geometric twist almost remained uniform in this region and this region would also be almost free of spanwise flow.

The finlets were rapid prototyped using ABS like material which resulted in slight flexibility which is beneficial during installation. The finlets were designed to be installed parallel to the flow and flush with the trailing edge of the wind turbine blade.

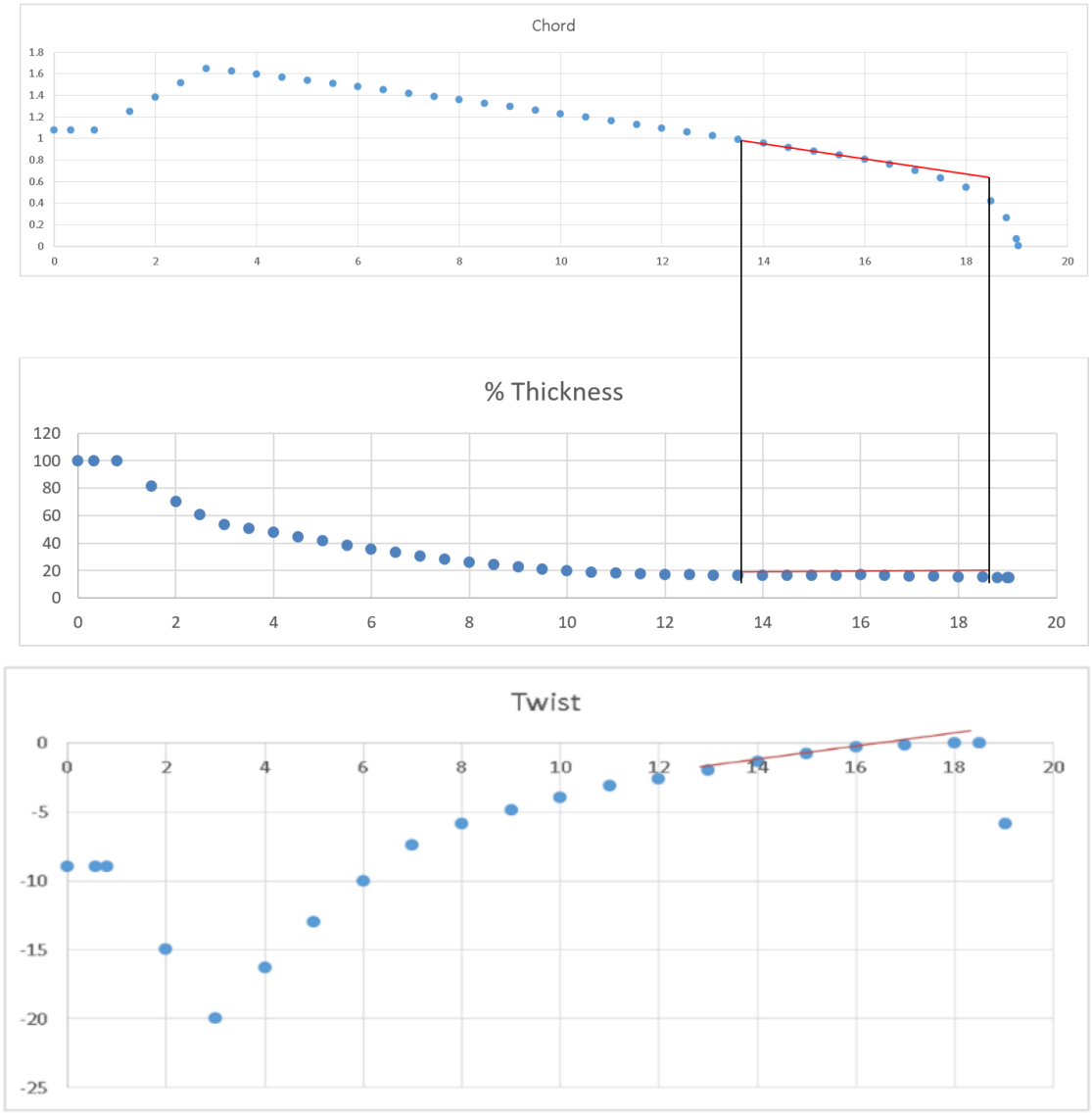

Figure B-22 - Chord, thickness and twist distribution of the Nordtank turbine blade.

References

[1] I. A. Clark, W. Devenport, J. W. Jaworski, C. Daly, N. Peake, and S. Glegg, “The Noise Generating and Suppressing Characteristics of Bio-Inspired Rough Surfaces,” *20th AIAA/CEAS Aeroacoustics Conf.*, no. June, 2014.

[2] I. A. Clark, W. N. Alexander, W. Devenport, and B. Raton, “Bio-Inspired Trailing Edge Noise Control,” *21st AIAA/CEAS Aeroacoustics Conf.*, no. June, pp. 1–18, 2015.

[3] I. Clark, D. Baker, W. N. Alexander, W. J. Devenport, S. A. Glegg, J. Jaworski, and N. Peake, “Experimental and Theoretical Analysis of Bio-Inspired Trailing Edge Noise Control Devices,” *22nd AIAA/CEAS Aeroacoustics Conf.*, 2016.

[4] Lilley, G., "A study of the silent flight of the owl", AIAA paper 98-2340, June 1998.